MOLECULAR DYNAMICAL SIMULATION OF METAL-CROSSLINKED HYDROGELS

by

Hang Tien Nguyen

B.S. in Mathematics and Computer Science, Vietnam National University at HCM, 2002

M.A. in Mathematics, University of Pittsburgh, 2015

Submitted to the Graduate Faculty of

the Dietrich School of Arts and Sciences in partial fulfillment

of the requirements for the degree of

Doctor of Philosophy

University of Pittsburgh

2019

UNIVERSITY OF PITTSBURGH

DIETRICH SCHOOL OF ARTS AND SCIENCES

This dissertation was presented

by

Hang Tien Nguyen

It was defended on

October 10, 2016

and approved by

David Swigon, PhD, Associate Professor, Department of Mathematics

Anna Vainchtein, PhD, Professor, Department of Mathematics

Tara Meyer, PhD, Professor, Department of Chemistry

Brent Doiron, PhD, Professor, Department of Mathematics

Dissertation Directors: David Swigon, PhD, Associate Professor, Department of Mathematics

and Anna Vainchtein, PhD, Professor, Department of Mathematics

MOLECULAR DYNAMICAL SIMULATION OF METAL-CROSSLINKED HYDROGELS

Hang Tien Nguyen, PhD

University of Pittsburgh, 2019

We develop a computational model to study the compaction, network topology and elastic response of hydrogel as a function of crosslink density. Our simulations start with a covalently bonded polymer network, to which we introduce additional crosslinks by binding metal cations to reactive groups distributed along the polymer chains. We find that these crosslinks increase the compaction of the polymer network in two ways: (i) by crosslinking neighboring groups on the same polymer chain and thereby shortening the effective length of polymer chains, and (ii) by linking together two or more distinct polymer chains. These two effects combine to overall hydrogel contraction and stiffening. Our results show that the elastic modulus of the hydrogel increases significantly due to the additional crosslinks, in agreement with recent experimental observations. With the help of computer simulations, we find the relations between parameters of our model and chemical characteristics of the hydrogel such as the modulus, the compaction of hydrogel, or the average number of reactive groups bound to a single crosslinker. We analyze geometric and topological characteristics of the hydrogel, such as the time evolution of distance between groups in the hydrogel, or the proportion of crosslinks that are retained, broken or newly formed during the course of simulations. These characteristics help us better understand the internal structure of the hydrogel and explain experimental observations such as the compaction of the hydrogel when metal crosslinkers are introduced. Despite its simplicity, the model qualitatively captures the important chemical properties of the crosslinkers.

TABLE OF CONTENTS

LIST OF TABLES

LIST OF FIGURES

ACKNOWLEDGEMENTS

I am deeply indebted to my advisors, David Swigon and Anna Vainchtein, for their many invaluable guidance, advice, and constant support over the years. They have spent a lot of time with me since the beginning of my study. In research projects, they explain the theories and practical methods of mathematical and computing modelling which were totally new to me, getting me practice with scientific writing and presenting.

For the research project related to this thesis, I truly thankful to the members of the Graphene group, especially to Tara Meyer and Jeffrey Auletta, for their enthusiastic and fruitful suggestions. I am very grateful to Brent Doiron and Tara Meyer for their careful reading of the thesis and for their serving in the thesis committee.

I wish to thank to the Department of Mathematics, to all the faculty, staffs and classmates for supporting me of my PhD study in University of Pittsburgh. In particular, I would like to thank Christ Lennard, Toan Nguyen, Jeromy Sivek and Tuyen Truong for their encouragement and constant help.

I am very grateful to my family who constantly support and believe in me. I would like to thank my former teachers for their encouraging and teaching me in mathematics. Many deep thanks go to my many friends for being my friends and helping me in life

1.0 INTRODUCTION

1.1 HYDROGEL: A HYDROPHILIC POLYMERIC NETWORK

A polymer is a very large molecule, made from many repeated units called monomers. Polymers can be found as naturally occurring materials such as DNA and natural rubber, or synthesized as chemical materials such as nylon and synthetic rubber. A polymer network is formed by crosslinking linear polymer chains, either permanently, via covalent bonds, or temporarily, via ionic bonds. Examples of some common crosslinkers for covalent bonds are bissulfosuccinimidyl suberate (BS3) used in protein studies or polyethylene glycol (PEG) used in various fields such as chemistry, medicine, biology, industry. The common crosslinkers for ionic bonds are metal ions such as Fe^{3+}, Fe^{2+} and Na^{+}.

A hydrogel is a hydrophilic polymeric network with significant water content. Chemical groups of a hydrogel are either ionizable or neutral. If a group can form a crosslink with a crosslinker, we call it a reactive group. Otherwise, it is a non-reactive group. Similarly to other polymers, hydrogels range from natural tissue such as collagen and fibrin to synthetic material such as polyvinyl alcohol. Hydrogels are capable of swelling/deswelling reversibly in water and retaining liquid in swollen state. Due to their unique properties including high water content, rubbery nature and permeability, hydrogels have been used in various pharmaceutical and biomedical applications [47, 69]. Swelling of a hydrogel loaded with a drug helps the polymer chains move further apart, so that the drug can diffuse more quickly [6, 71]. Hydrogel is moist, soothing and easily removed, so it is a good material for wound dressing [81]. Hydrogels are used widely in tissue engineering because they can resemble natural living tissue more than any other class of synthetic biomaterials [16, 91] . Other applications of hydrogels include soft contact lenses [82], hygienic products [6],

coal dewatering [97].

1.2 SIMULATIONS OF POLYMER NETWORKS

1.2.1 Polymer models and simulation methods

Various methods have been developed to model the behavior of permanently crosslinked polymer networks [10, 25, 30, 34, 54, 56, 85]. Polymer models are classified in two different groups: coarse-grained and atomistic [10, 54, 56]. Coarse-grained models are simplified descriptions in which some degrees of freedom have been integrated over [54]. In these models, chemical groups of monomers or the entire monomers are modeled as a single entity. Some well-known examples of coarse-grained models of polymer chains are freely-jointed chain or bead-spring chain [54]. With coarse-grained models, people can study properties that are independent of chemical structures of monomers, such as the effects of chain topology or bond flexibility on polymer network behavior.

In the more realistic atomistic models, each atom and covalent bond is treated as a separate entity. Atomistic models account for the details of chemical structures of polymers. Atomistic models are usually employed to study particular properties of particular polymers. Such models are commonly used in applications to medicine and biology. Using atomistic models requires a large simulation time scale and involves many features of polymers at the atomic level such as topology and molecular structure. Due to this complexity, much of the work has been devoted to developing coarse-grained models for a variety of polymers, proteins or nucleic acids [10, 44, 85].

Early polymer chain investigations involved analytical methods and were based on coarse-grained models. This includes derivation of the partial differential equations describing, for example, the polymer density, based on laws of polymer physics and statistical mechanics. Some commonly used models can be found in [25, 30, 34]. Analytical methods for polymer networks are usually based on lattice models [54]. For instance, Flory-Higgins polymer theory describes the

excess energy and entropy in a lattice-based mean field theory. Though lacking many details, these theories can predict many physical properties of polymer networks and solutions such as chain length or stiffness of polymer.

These theoretical approaches cannot be used to describe details such as bonding interactions or structural characteristics of a polymer network. To study coarse-grained and atomistic models more directly and efficiently, one can employ numerical simulations. In particular, simulation methods are often used to find the equilibrium states of polymer networks and to calculate and analyze their thermodynamics properties. Among the important properties of polymers, much of the focus is on studying their elasticity, i.e., the ability of a material to resist a distorting stress without breaking and to return to its original size and shape when the stress is released.

One common approach to simulate the behavior of polymer networks involves Monte Carlo (MC) methods with the bond fluctuation model in a lattice or in continuum space [1, 17, 23, 25, 42, 89]. In MC simulations, the successive configurations of the system are independent identically distributed random variables sampled from a distribution that describes the probability of their occurrence. The method has been used to simulate the equilibrium of unstressed or deformed hydrogel network [19, 63], but not dynamical changes in the network configuration.

Molecular modelling [31, 54] allows one to investigate the behavior of polymer networks more efficiently. In molecular simulation methods, interaction potentials and topological properties of the polymer networks are used as inputs. The interaction potentials include bonded interactions between atoms connected by covalent bonds, and non-bonded interactions between atoms of chains, or between atoms of the same chains but not connected by covalent bonds. The configurations of the system then are usually generated either using MC or dynamics methods which are based on mathematical models of dynamics of the polymer. The two most popular dynamics methods are Molecular Dynamics (MD) and Brownian Dynamics (BD).

MD methods are based on numerical solution of the classical equations of motion. In contrast to MC methods, MD simulations also provide information about the time evolution of the system. MD simulations reveal more details about the topological and geometrical properties of the

networks and time evolution of physical properties such as stress tensor and kinetic energy [108-109], which can be used to predict the properties of polymer network and to improve the model. In recent MD simulations, the authors have used either the optimized interatomic force fields [12] that are built in the various MD simulation software, or specially defined interactions [39, 108-109]. In [39], a harmonic-like potential with a cutoff was used as an attractive potential, and in [108-109], the authors used a Morse-type potential to simulate the permanent polymer networks.

Brownian Dynamics (BD) [24, 27, 28, 55], also known as Langevin Dynamics, is a simulation method similar to MD, but based on the Langevin equation of motion instead of classical equations of motion. In BD, a particle is subjected to a random force from many collisions with solvent molecules, and a friction force proportional to the particle's velocity is applied to the solvent [54].

The MC method does not describe the dynamical evolution of the system, but it samples configurations much more efficiently and, as a result, the system reaches its equilibrium states much quicker than in MD and BD simulations. For this reason, the MC method is often the preferred choice for molecular simulations. When the running time of simulation is reasonable and a detailed analysis of the topological structure and time evolution of the physical properties of the system is needed, a dynamics simulation method is typically employed. In the cases, MD is usually the preferred method, while BD is useful for polymer simulations that focus on the effects of solvent.

There are many applications of polymer simulations in industry [32, 73, 84, 92]. Many polymer properties (such as diffusion coefficients) can now be estimated with sufficient accuracy if properly parameterized [107]. Results of many polymer simulations using molecular dynamics can be compared to experimental data and used to design new materials [102, 107] such as polymer membranes and permeation [84, 92].

1.2.2 Simulations of hydrogels

As mentioned above, one of the remarkable properties of a hydrogel is its ability to swell/deswell reversibly in water and retain liquid in the swollen state. Hydrogels respond to a variety of physical

and chemical stimuli from the environment such as temperature, electric current, pressure, magnetic field, pH and salt concentration of the solvent, etc., and may change their volume as a result. Most hydrogel simulations focus on the study of the swelling/deswelling behavior of hydrogels in different environments. In the simulations, other characteristic quantities such as elastic modulus are also analyzed.

In recent years, there have been a lot of advances in understanding the swelling behavior of hydrogels using molecular simulations. In these simulations, various models are used to include the effect of water molecules inside and outside of the hydrogel [56]. Atomistic simulations can be used to understand the details of interactions between the polymer and the solvent of some particular hydrogel [3-5, 20, 75-76, 99, 104]. However, atomistic simulations for polymers larger than 50 monomers are too expensive. This scale limitation makes it difficult to compare the simulation results quantitatively with experimental observations. In coarse-grained models, the dynamics of the solvent is treated implicitly in several ways. For instance, it may be represented as a dielectric continuum [56] with a given permittivity or by frictional and random forces (as

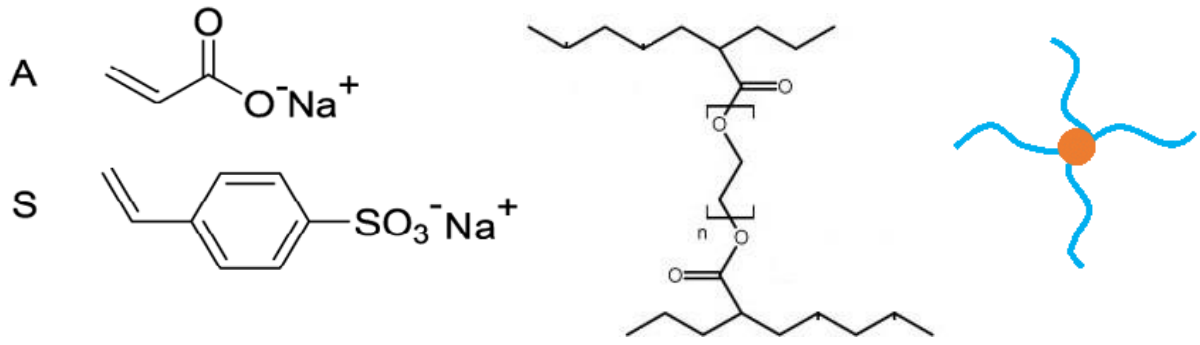

(a) (b) (c)

Figure 1.1. The structure of the polymer. (a) The chemical structures of A and S (b) PEG-DA structure and crosslinking (c) 4 arms PEG-DA

mentioned in the previous section). Simulations of the coarse-grained models can be conducted on longer time scales and for larger system sizes. These models reveal the effects of chain length,

crosslink density, fraction of charged monomers or the swelling/deswelling behavior of the hydrogel in experiments [56].

1.3 EXPERIMENTAL MOTIVATION

1.3.1 Experimental studies of hydrogels with metal crosslinks

Experiments show that hydrogels exhibit a change in volume and elastic modulus in response to addition of metal crosslinkers [8, 74, 77]. The evolution of volume and modulus depends on the metals and the hydrogel, as well as the environmental factors such as pH.

In this thesis we develop a model of the hydrogel specific to experiments described in [8]. This hydrogel consists of linear chains of sodium acrylate (reactive group A) and sodium 4-styrenesulfonate (non-reactive group S) (see Figure 1.1a) in a mole ratio of 1:1 crosslinked permanently by polydiacrylate (PEG-DA, see Figure 1.1b). The hydrogel is electroresponsive in that it can be tuned reversibly between hard and soft states by adding metal cations. Specifically, upon the addition of Fe^{3+} or Fe^{2+} to the hydrogel, A groups can form additional strong crosslinks via Fe^{3+} and weak crosslinks via Fe^{2+} [8]. Experimental results in [8] show that the elastic modulus of the hydrogel increases significantly with addition of Fe^{3+} but not with Fe^{2+} (see Figure 1.2). In the experiments, the ratio of Fe^{3+}/Fe^{2+} is varied while the total molar concentration of Fe^{3+} and Fe^{2+} is fixed at 0.5 M.

1.3.2 Internal structure of the hydogel

The characteristic quantities of the hydrogel studied in [8] include the **coordination number** of a crosslinker, which is defined as the number of reactive groups A bound to that crosslinker, and the number of **complex components**, which are formed when A groups bound to two or more crosslinkers. Another important quantity is the number of **bridging crosslinkers**, i.e., the crosslinkers that are bound to two or more different chains, and the size of the **loops**, which are

formed when crosslinkers bound to two A groups of a single chain. In what follows, a loop is considered **long** if it contains more than five polymer units. Otherwise, it is called a **short** loop.

In polymer theories, **crosslink functionality** is defined as the number of chain arms (see Figure 1.1c) bound to a PEG-DA. Crosslink functionality is not fixed across the hydrogel [61]. In this thesis, the maximum of crosslink functionality is four [9].

The size a group S is roughly double the size of a group A and is much larger than Fe ions [9].

Besides these important geometric and topological network properties, there are many other chemical properties which are observed in the experiments as follows [8-9]:

- Both the addition of Fe^{3+} and Fe^{2+} cause the hydrogel to shrink, but the decrease in swelling is much larger for Fe^{3+}.
- While the expectation of the maximum coordination number of the iron ions with singly charged carboxylate (chemical compound contained in group A) anions is equal to their oxidation state, 2 or 3, complexes (with coordination numbers that vary from zero to five, and are mainly in the range from two to four) can be considered chemically reasonable.
- Under the experimental conditions, the binding constant of the Fe^{2+} was shown to be very small, consistent with very weak crosslinking. This implies that the average coordination number of Fe^{2+} is very small.
- There are complex components in the hydrogel.

1.4 THE OBJECTIVES OF THIS THESIS

To our knowledge, effect of metal crosslinkers on elastic properties of hydrogels has not been previously modeled. Until recently, experimental information necessary to model the effect of metal crosslinks on stiffness of hydrogel has been lacking.

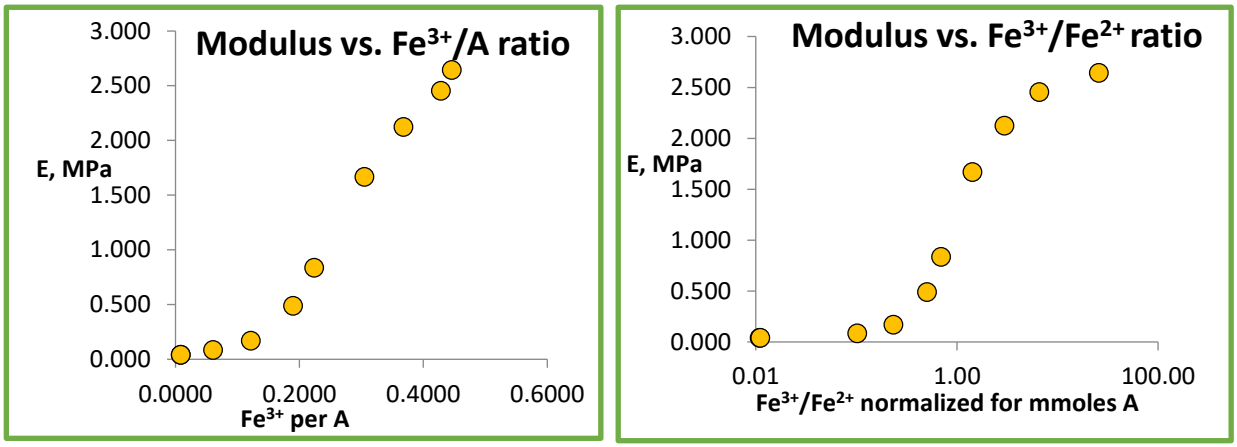

(a) (b)

Figure 1.2. Stiffness of the hydrogel with different proportion of Fe^{3+}/A or Fe^{3+}/Fe^{2+} in experiments [8-9].

In this thesis, we introduce a model of hydrogel that aims to capture and explain some of the experimental findings in [8] which we described in Section 1.3. We build a coarse-grained model of the hydrogel based on the network properties discussed in Section 1.3 and study it using MD simulations. By calculating and analyzing the characteristic quantities we match the results in the simulations qualitatively to those in experiments and explain which features of the network have the largest influence on the experimental observations.

1.5 SUMMARY OF THE THESIS

To better understand the elastic response of the hydrogel as a function of crosslinker density and other properties, we develop and study a computational model that accounts for both permanent (covalent) and temporary (metal) crosslinks. The model presented here extends the work of Wu, Li and Nies [108-109], where MD simulations with Morse-type interactions are used to describe formation and mechanical properties of a polymer network. In [108-109], the authors provided a method to simulate a polymer permanent networks with a given maximum crosslink functionality.

They also analyzed the elasticity of the permanent networks.

In developing the model, we closely collaborated with the authors of [8]. They were the members and collaborators of Meyer group (University of Pittsburgh, 2015). The authors, in particular J. T. Auletta and T.Y. Meyer, provided not only detailed information about the volume and modulus dependence on the metal crosslinker fraction but also values of some characteristic quantities of the internal hydrogel structure which they estimated from the results [9]. We used this information to develop and evaluate our model.

Our main focus is on the understanding of the effect of metal crosslinking on the internal structure and elastic properties of the hydrogel. The present study aims to investigate the evolution of the elastic modulus, the characteristic quantities mentioned in Section 1.3.2 and other topological and geometries properties of polymers such as the distance between groups. For these reasons, a dynamics simulation method is more suitable than MC. Since the study does not focus on the effect of the solvent on the system, MD simulations are used, as in [108-109].

We first simulate the formation of the covalently bonded polymer network and analyze its properties. Then we add metal crosslinkers to the hydrogel. The overall number of Fe ions is fixed but the Fe^{3+}/Fe^{2+} fraction is varied in different simulations, and consequently Fe^{3+}/A fraction varies as well. Our model captures well the dependence of compaction and stiffness of hydrogel on the valence and concentration of crosslinkers. By observing the dynamics of the formation of additional crosslinks formed by the bonds between Fe^{3+} and A, we analyze the connectivity of the network and other properties as functions of Fe^{3+}/Fe^{2+} or Fe^{3+}/A fractions.

In our model, **a type of crosslinker** is defined by interaction potentials between crosslinkers and groups in the hydrogel or between crosslinkers themselves. If some of these potentials change, we have a **different type of crosslinker**. Crosslinkers of different types result in different characteristic quantities of the hydrogel. We present two models of hydrogel which account for different types of metal crosslinkers and the same covalent network.

To explain the properties and understand the internal structure of the simulated hydrogel, we calculate the characteristic quantities such as the number of bridging Fe, number of loops, the

average distance between groups or number of units of an **effective chain**. Here, an effective chain is a chain segment in which the monomers can be considered freely joint. We also monitor the change of the characteristics during the simulation by analyzing their time evolution.

In the Model I, we simulate Fe^{2+} as neutral atoms, i.e., we assume that they do not bind to A groups. This means that in Model I, the only additional crosslinker is Fe^{3+}. Model I does not reflect some properties in [8] such as the compaction of hydrogel when Fe^{2+} is added [8]. However, by analyzing the characteristic quantities in the Model I as below, we understand the factors that change the characteristic quantities such as the modulus or the size of the hydrogel.

To understand why the elastic modulus increases with the proportion of Fe^{3+}/A, we used Model I to investigate the effects of bound Fe^{3+} and bridging Fe^{3+} on the elastic modulus of the hydrogel. We found that the effective length of the chains becomes shorter as the density of Fe^{3+}/A increases. The percentage of crosslinked-chains and the number of chains bound to a single chain each increase with the Fe^{3+}/A fraction. Both the shortening the effective chains and the crosslinking of the chains of the permanent network make the hydrogel stiffer, but the Model I shows that the significant increase of modulus is due to the crosslinking of the chains. We also find that the number of bridging Fe^{3+}, the number of long loops and number of short loops are the factors affecting to the compaction of the hydrogel.

Based on Fe^{3+} crosslinkers in Model I, we construct a model of hydrogel in which both Fe^{3+} and Fe^{2+} can bind to A group, with the goal of capturing properties observed in the chemical experiments we mentioned in Section 1.3. This model is referred to as Model II. Computer simulations reveal the relations between some parameters in our model and some characteristic quantities such as the modulus, the compaction of hydrogel, or the average coordination number of crosslinkers. This information enables us to simulate different types of crosslinkers to obtain the values of characteristic quantities we want to capture. We then select suitable parameters of Fe^{3+} and Fe^{2+} for the Model II. The Model II captures qualitatively all hydrogel properties we discussed in Section 1.3 except that the average coordination numbers of Fe^{2+} is not sufficiently small. Although the average coordination number of Fe^{2+} in Model II is smaller than the one of

Fe^{3+}, it is still relatively large compared to the experimental results [8-9]. Analyzing the Model II, we find that the significant increase of the hydrogel modulus is due to the bridging crosslinkers, and most of them are Fe^{3+}.

In conclusion, the two models suggest that the elastic and compaction response of the hydrogel in the experiments [8] could be explained by the change of hydrogel network due to metal crosslinks. In particular, the bridging Fe^{3+} crosslinkers are primarily responsible for the significant increase of the hydrogel stiffness.

1.6 OUTLINE OF THE THESIS

Our thesis consists of seven chapters. The rest of the thesis is organized as follows.

The second chapter describes the model, simulation processes, the formation and solution of classical equations of motion. It includes the descriptions of interaction potentials and their parameters for the covalent network and Model I. In this chapter, we present the methods and algorithms that are used to model temperature and pressure of the hydrogel.

In Chapter 3 we present the results of simulations of the formation process of permanent hydrogel network, which is common for both Model I and II. Then we analyze the nonlinear elasticity of the hydrogel in the absence of metal crosslinkers.

In Chapter 4 we present the Model I (in which Fe^{2+} cannot bind to A groups but Fe^{3+} can bind strongly). We analyze the probable causes of the decrease of the size and significant increase of the elastic modulus of the hydrogel as Fe^{3+}/A fraction increases. We also analyze the topological characteristics of the network such as the coordination number of Fe^{3+} or the complex components.

In Chapter 5 we construct Model II (in which both Fe^{3+} and Fe^{2+} can bind to A groups). We study the correlations between the parameters of interaction potentials and values of characteristic quantities. This enables us to find suitable values of parameters for crosslinkers to obtain the values

of characteristic quantities qualitatively similar to the results in the experiments. We choose suitable values of parameters of Fe^{3+} and Fe^{2+} for Model II.

In Chapter 6 we present the results for Model II. We analyze the hydrogel by calculating the characteristic quantities similarly to Model I. We also compare the characteristic quantities of Fe^{3+} and Fe^{2+}.

In Chapter 7, we summarize and discuss our results and future work, and provide conclusions.

The supplementary material comes after Chapter 7. It consists some supporting material we used for running the simulations in the thesis including the Matlab code to generate the tables of interaction potentials, the MD run parameters for the simulation steps and the topological parameters of the initial system.

2.0 SIMULATION PROCESS

2.1 THE MODEL OF HYDROGEL NETWORK AND CROSSLINKER

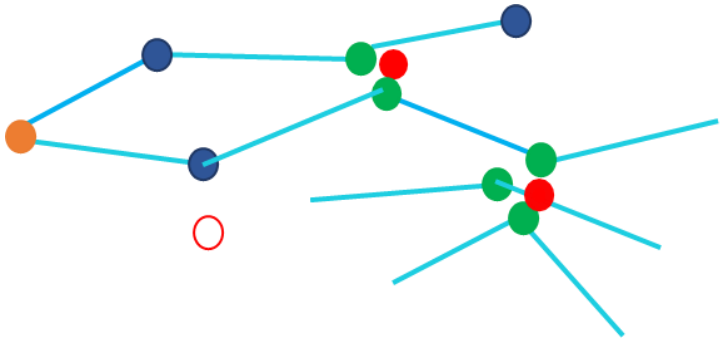

Figure 2.1. The model of the hydrogel. The mass centers of A group, S group, PED-DA group, $Fe^{3+}$and Fe^{2+} are presented by the green, blue, orange, solid red and hollow red points, correspondingly. The cyan lines are the segments connecting two groups.

In our model, the hydrogel studied in the experiment we are considering [8] is represented as a 3D network of chemical groups connected by bonds that are governed by interaction potentials introduced below. Each chemical group or atom (S, A, PEG-DA, Fe^{3+} or Fe^{2+}) is represented by a point mass (see Figure 2.1). We do not account for the exact sizes of the groups but we use their physical properties as a guide in designing the qualitative phenomenological potentials governing their interactions. We model the hydrogel at the mesoscale level as a periodic medium, with each unit cell containing N = 250 precursor linear chain segments, formed by m = 40 connected A (green) or S (blue) groups.

These chain segments are connected at their ends to a PEG-DA (orange) group, modeling the

permanently crosslinked hydrogel. Once formed, these bonds are treated as covalent bonds for the duration of the simulation. We present two models of hydrogel which differ in the interactions between metal crosslinkers and the rest of the network. The covalently bonded network is assumed to be same in both cases. In Model I, we choose interaction potentials for metal crosslinkers so that Fe^{3+} (solid red) can form strong bonds with the A groups, while Fe^{2+} (hollow red) does not bind at all. On the other hand, in Model II, both Fe^{3+} and Fe^{2+} can bind to A groups but the bonds between Fe^{3+} and A are stronger. Model I is based on the assumption that Fe^{2+} ions do not bind to A groups. It captures all other important experiment results in [8-9] but does not reflect the compaction of hydrogel when we add Fe^{2+}. Model II improves this aspect but the coordination numbers of Fe^{2+} are relatively large compared to the results in [8-9].

As in Wu et al. [108-109], the interactions between the different chemical groups and ions (A, S, PEG-DA, Fe^{3+} and Fe^{2+}) in the system are characterized by pairwise potential functions. We consider the interactions between chemical groups to be one of four types: *covalent (permanent) bonds, crosslinking (reversible) bonds, steric repulsions and bond angles*. These phenomenological potentials are calibrated to mimic the effects of such chemical features as charge, polarization, presence of water, hydrophilicity, etc. The values of parameters in this section are specific for the covalently bonded network and the Model I. We select them roughly based on the [108-109] and some expected physical properties of groups and atoms observed in simulations. In Chapter 5, based on the relation between parameters and characteristic quantities from computer experiments, we will select the suitable values for the Model II.

2.1.1 Covalent bond potential

The precursor linear polymer chains consist of A and S groups connected by harmonic bonds with the harmonic potential between any two groups given by

$$V_{bond}(l) = \frac{1}{2}k_b(l - l_0)^2 \tag{2.1}$$

In our simulations, the value of k_b for all covalent bonds is set to be 3.76 x 10^5 kJ mol^{-1} nm^{-2}, which is the same as the value used previously by Wu et al. in [108-109]. The parameter $l_0 =$ 0.153 nm is the equilibrium length of the bond. The instantaneous bond length l is determined by the distance between the two interacting groups. The PEG-DA bonds with A and S are governed by the same interaction potential.

2.1.2 Steric repulsion

All non-bonding interactions are repulsive and are governed by the Weeks-Chandler-Andersen (WCA) potential [29], which is defined as the Lennard-Jones potential with a cutoff:

$$V_{WCA}(r) = \begin{cases} \varepsilon\left(1 + \left(\frac{r_{PQ}}{r}\right)^{12} - 2\left(\frac{r_{PQ}}{r}\right)^{6}\right), & r < r_{PQ} \\ 0, & r \geq r_{PQ} \end{cases}, \quad (2.2)$$

Here r_{PQ} is the equilibrium distance of the WCA potential, which depends on the groups P and Q, r is the instantaneous distance between the two interacting groups, and ε =0.391 kJ mol^{-1} (as in [108-109]) is the depth of the WCA potential. The WCA potential introduces a strong repulsion between the groups P and Q if the distance between them is less than r_{PQ}. We calibrate the value of r_{PQ} between any pair of groups in such a way as to take into account the relative sizes of the groups and the presence of any other additional repulsive forces, such as electrostatic, or polar interactions. We use the value of $r_{PQ} = 0.45$ nm as in [109] for the interaction between A-S and S-S. In order to reflect the smaller size of A relative to S [9], we use $r_{PQ} = 0.3$ nm for A-A interactions. The Fe group consists of a single atom, and hence we choose $r_{PQ} = 0.22$ nm for S-Fe and 0.12 nm for A-Fe interaction. For the interaction between two Fe groups, we choose a larger value for r_{PQ} than would be implied by their size in order to account for the electrostatic repulsion due to their positive charge and set $r_{PQ} = 0.45$ nm. Finally, the sizes of S and PEG-DA groups in the hydrogel are comparable and they both do not form bonds with Fe^{3+}. Therefore, in our simulations we set $r_{PQ} = 0.45$ nm for PEG-DA and S groups.

2.1.3 Crosslinking bond potential

The bonding interaction between the crosslinkers and the reactive groups in our model is governed by the Morse potential

$$V_{Morse}(r) = D\left(e^{-2\beta(r-b)} - 2e^{-\beta(r-b)}\right) \tag{2.3}$$

where r is the distance between the crosslinker and reactive group, b is the equilibrium distance, D presents the maximum of Morse potential, while β controls its flexibility, i.e., the distance over which the potential is effective. A larger value of β makes the effective distance shorter. The force formed from the Morse potential introduces a strong repulsion between the crosslinker and reactive group if the distance between them less than b. So in a short range, the Morse potential also mimics the steric repulsion similarly to the WCA potential. Thus, when selecting the value of b of two interacting groups, we need to consider their relative sizes. If the distance between the crosslinker and reactive group larger than b, the force of Morse potential is attractive.

Both D and β affect the attractive force. Given values of D and b, the larger β make the attractive force stronger in its effective range. And given values of β and b, a larger value of D makes the attractive force stronger.

In our model, we consider a crosslink between A group and a Fe^{3+} atom to be formed when the distance between the point masses representing them is less than $b + \ln(2)/\beta$, the value at which the attractive force corresponding to the Morse potential attains its maximum value $D\beta/2$.

There are different values of D and b chosen to correspond to (i) the permanent connection between PEG-DA with A, and (ii) the temporary crosslinking between A and ions. For PEG-DA-A, we assign the value D=150 kJ/mol and b =0.15 nm, as in [108], while for A-Fe^{3+} in Model I, we set D = 90 kJ/mol and b =0.12 nm.

The parameter β controls the effective distance of the potential and determines the coordination number of crosslinkers. The parameters are selected to produce an average coordination of 2 to 4 and a maximum of 6. Based on trial simulations, we set β = 15 nm^{-1} for A-Fe^{3+} interaction in

Model I. In the permanent network formation simulation, where a maximum "coordination" of 4 is targeted, we set β = 60 nm^{-1} for PEG-DA-A as in [108].

2.1.4 Bond angle potential

We also include bond angle potential as in [109]. We use the cosine-based harmonic potential to model the constraint of the bond angles. Let us consider a triple of groups r_α $(\alpha = i, j, k)$ such that group pairs (i, j) and (j, k) are covalently connected and the bond angle $i - j - k$ is θ. Then the interaction potential between the three groups is:

$$V_a(\theta) = \frac{1}{2} k_a (\cos(\theta) - \cos(\theta_0))^2 = \frac{1}{2} k_a \left(\frac{r_{ij}^2 + r_{kj}^2 - r_{ik}^2}{2 r_{ij} r_{kj}} - \cos(\theta_0) \right)^2 \tag{2.4}$$

In (2.4), k_a is the angle bending force constant and θ_0 is the equilibrium angle. We use the value of k_a = 568.5927 kJ/mol and θ_0 = 110^o, as in [109].

2.1.5 Summary of parameters

The parameters of all interaction potentials for permanent network and Model I are summarized in Table 2.1.

The mass of each group is the same for the two models: $m_A = 72$ u, $m_S = m_{PEG-DA} = 183$ u, $m_{Fe^{3+}} = m_{Fe^{2+}} = 55.8$ u [9].

2.1.6 Governing equations

The potential energy V of the system of N interacting groups, a function of positions $r_i = (x_i, y_i, z_i)$ of all groups, is defined by the sum of all interaction potentials. For our model, the potential energy of the hydrogel is

$$V(r_1, \dots, r_N) = \sum_{bonds} V_{bond} + \sum_{angles} V_a + \sum_{pairs} V_{WCA} + \sum_{pairs} V_{Morse} \tag{2.5}$$

Table 2.1. Parameters of the interaction potentials for permanent network and the Model I

Harmonic Bond	k_b (kJ mol^{-1} nm^{-2})	l_{PQ}(nm)
A-A	376141.6	0.153
A-S	376141.6	0.153
S-S	376141.6	0.153
WCA	ε (kJ mol^{-1})	r_{PQ} (nm)
S-S	0.391	0.45
A-S	0.391	0.45
A-A	0.391	0.3
A-Fe^{3+}	0.391	0.12
A-Fe^{2+}	0.391	0.12
S-Fe^{3+}	0.391	0.22
S-Fe^{2+}	0.391	0.22
Fe^{3+}- Fe^{3+}	0.391	0.45
Fe^{3+}- Fe^{2+}	0.391	0.45
Fe^{2+}- Fe^{2+}	0.391	0.45
PEG-DA-S	0.391	0.45
PEG-DA-A	0.391	0.45
PEG-DA- PEG-DA	0.391	0.45
PEG-DA- Fe^{3+}	0.391	0.22
PEG-DA- Fe^{2+}	0.391	0.22
Morse	D (kJ mol^{-1})	β (nm^{-1})	b (nm)
Fe^{3+}-A	90	15	0.12
PEG-DA-A	150	60	0.15
Bond Angle	k_a(kJ mol^{-1})	θ_0 (degree)
Any consecutive segments	568.5927	110

In the first and second term, the summation indices run over all the bonds, angles of the covalent network of the hydrogel, whereas in the last two terms the summation indices run over all the pairs of groups whose interaction is governed by the WCA and Morse potentials, respectively.

The force acting on group i is given by

$$F_i = -\nabla_{r_i} V(r_1, \dots, r_N) = -\left(\frac{\partial V}{\partial x_i}, \frac{\partial V}{\partial y_i}, \frac{\partial V}{\partial z_i}\right) \tag{2.6}$$

The core of a molecular dynamics simulation is the solutions of the classical equations of motion for all groups in the system. The classical equations of motion for this system can be formulated in several ways such as Newtonian, Lagrangian or Hamiltonian. Here we present the Newtonian form:

$$m_i \frac{\partial^2 r_i}{\partial t^2} = F_i, \quad i = 1 \dots N \tag{2.7}$$

2.1.7 Solvation model

Since our main goal is to analyze the effects of metal crosslinks between Fe ions to A groups on the elastic behavior of the hydrogel, the interactions between water and the groups in the system are not described in detail by our model.

To be more specific, we do not explicitly simulate water in the hydrogel. However, there are some factors that reflect the presence of water. First, to mimic steric repulsion between particles, we use WCA potential which includes only short range repulsive interaction. In liquid, WCA is more suitable than Lennard-Jones potential which includes both short range repulsion and long range attraction [106].

We also simulate the presence of water by fixing the volume of the simulation cell when relaxing or deforming the hydrogel (see Sections 2.3.1.3 and 2.3.4) and by fixing the pressure imposed on the simulation cell when water is expected to be drawn in or pushed out. When the volume of the hydrogel changes due to pressure, the value of compressibility is set to be the compressibility of water (see Section 2.3.1.2). Therefore, our models also reflect the presence of

water when the volume of the hydrogel changes.

2.2 SIMULATION PACKAGE

To produce the simulations of the hydrogel, we use GROMACS 4.6 software [41]. Due to its algorithm and processor optimization, GROMACS is one of the fastest molecular dynamics simulation software packages [40, 57]. GROMACS is a popular choice among many similar software packages because it offers a lot of simulation tools such as multiple options for numerical solvers, commonly used force fields, temperature and pressure coupling methods and simulation options such as user defined potential, Langevin dynamics, etc. In our simulations, we utilize the MD integrator which uses the leapfrog method for solving the Newton's equations of motion. For the non-bond interaction of the force fields, GROMACS offers Morse potential but not WCA potential. We implement all the non-bond potentials (Morse and WCA) by creating tables for user-defined potentials.

2.2.1 Algorithm for solving dynamical equations

There are various methods to numerically solve equations (2.5)-(2.7). In our simulations, we use the leapfrog integration [13, 41], which is also the default algorithm in GROMACS to solve the dynamics equations. The method is symplectic, which means that it preserves the structure and conserves the energy of a Hamiltonian dynamical system.

For time step Δt, it updates positions r and velocities v using the forces $F(t)$ determined by the positions at time t by the formula:

$$v\left(t+\frac{1}{2}\Delta t\right) = v\left(t-\frac{1}{2}\Delta t\right) + \frac{\Delta t}{m}F(t) \tag{2.8}$$

$$\mathrm{r}(\mathrm{t}+\Delta t) = r(t) + \Delta t\, v\left(t+\tfrac{1}{2}\Delta t\right) \tag{2.9}$$

Based on positions and velocities, other thermodynamic quantities such as kinetic energy, temperature, pressure, etc. can be determined [41].

2.3 SIMULATION AND ANALYSIS METHODS

2.3.1 Simulation methods

The classical Hamiltonian equations of motion (2.5)-(2.7) describe a system with constant *number* of groups, constant *volume* and constant *energy* (NVE simulation). In practice, we usually need to simulate the system while maintaining a target temperature or pressure instead of energy.

2.3.1.1 Temperature coupling There are several methods to simulate a target temperature for a system [41, 54]. In our simulations, we use the Berendsen thermostat to mimic the temperature coupling. In this method, we force the system obey the equation

$$\frac{dT}{dt} = \frac{T_0 - T}{\tau} \tag{2.10}$$

Here τ is time constant for coupling. In our simulation, we use τ= 0.1 ps as in [108].

The absolute temperature is obtained using

$$T = 2\frac{E_{kin}}{(3N-3)k} \tag{2.11}$$

where $E_{kin} = \frac{1}{2}\sum_{i=1}^{N} m_i v_i^2$ denotes the total kinetic energy of the N-groups system and k is Boltzmann's constant.

To obtain the target T_0 at equilibrium states, for the simulation step n_c, after calculating the velocities v by (2.8), we need to rescale v to λv [11, 41] with

$$\lambda = \left(1 + \frac{n_c \Delta t}{\tau}\left(\frac{T_0}{T\left(t - \frac{1}{2}\Delta t\right)} - 1\right)\right)^{\frac{1}{2}} \tag{2.12}$$

2.3.1.2 Pressure coupling Similarly to temperature coupling, we use Berendsen barostat for our pressure coupling. The equation is

$$\frac{dP}{dt} = \frac{P_0 - P}{\tau_P} \tag{2.13}$$

Here τ_P is time constant for pressure coupling. In our simulation, we use τ_P= 1 ps as in [108].

GROMACS calculates the pressure P by first calculating the pressure tensor $\mathbb{P}$

$$\mathbb{P} = \frac{1}{V}\left(\sum_{i=1}^{N} m_i v_i \otimes v_i + \sum_{i<j}^{N} \mathbb{r}_{ij} \otimes F_{ij}\right) \tag{2.14}$$

where $u \otimes v$ denotes the direct product of two vectors u and v: $(u \otimes v)_{\alpha\beta} = u_\alpha v_\beta$, $\mathbb{r}_{ij} = r_j - r_i$, and F_{ij} is the force on group i exerted by group j. The force $F_{ij} = -V'_{ij}(r_{ij})\frac{\mathbb{r}_{ij}}{r_{ij}}$, in which V_{ij} is the total potential energy of the two interacting groups i and j, and r_{ij} is the distance between i and j.

The pressure then is obtained by using the formula

$$P = \frac{1}{3} trace(\mathbb{P}) \tag{2.15}$$

To obtain the target P_0 at equilibrium states, for the simulation step n_P, after calculating the positions r by (2.8) and (2.9), we need to rescale the positions and the simulation cell b to μr and μb, correspondingly [11, 41], with

$$\mu = 1 - \frac{n_P \Delta t}{3\tau_P}\gamma(P_0 - P) \tag{2.16}$$

where γ is the compressibility. In our simulations, γ= 4.5x10^{-5} bar^{-1}, which equals to the compressibility of water.

During simulations with pressure coupling, the coordinates and the simulation cell are rescaled by the same coefficient μ, so we can use the proportional change of the simulation cell in order to understand the proportional change of the hydrogel.

2.3.1.3 NVT and NPT simulations Two basic types of simulations of a simulation cell with periodic boundary conditions can be performed: NVT, where the *number* of molecules, *volume* of the simulation cell and *temperature* are fixed; and NPT, where the *pressure* is fixed instead of the volume. We produce NVT simulation by applying the temperature coupling mechanism described in Section **2.3.1.1**. NVT simulations are used to relax and mix the system before simulating any binding processes. The fixed volume in this type of a simulation mimics the presence of water and the resulting volumetric incompressibility of the hydrogel. NVT simulation is performed before and after network formation as well as after metal crosslinking simulation and deformation processes, as described below. NPT simulations are produced by combining the temperature coupling and pressure coupling (see Section **2.3.1.2**) mechanisms. NPT simulations are used for processes that change the volume of the system. This includes binding processes between the reactive groups and crosslinkers, or when properties of some groups are changed, e.g. when we replace some A by S, or add a permanent harmonic bond between two groups. In those kinds of processes the volume of the system changes in response to formation or breaking of bonds, or changes in potentials. In all NPT simulations, we set the reference pressure at 1 bar. The temperature in both NVT and NPT simulations is set to 300 K. The time steps for NVT and NPT simulations are 0.02 ps and 0.01 ps, respectively, as in [**108**]. The duration of each simulation depends on the time required to reach an equilibrium state. It is selected to ensure the stable state of the properties of the hydrogel such as the potential, the pressure, the temperature, size of the hydrogel, etc., at the end of an NVT or NPT run.

2.3.2 Permanent network formation

We begin our study by forming of the hydrogel network from precursor linear chains using a procedure similar to that employed in [108-109]. We start with 250 PEG-DA crosslinkers, and 250 linear chains, each containing 20 units of A and 20 units of S (this choice is based on the mol ratio that was mentioned in Section 1.3.1), randomly distributed with S placed at both ends of each chain. These chains are randomly placed in a cubic simulation cell with side of length 10 nm, with

periodic boundary conditions. At this step, only the two end groups of each chain are set up to be reactive via Morse potential with PEG-DA, in order to simulate the formation of a polymer network. As we allow for up to four interactions, network formation is expected. First, we run NVT simulation for 200 ns to equilibrate the system. During this run, S, A, and PEG-DA interact only via the WCA potential.

After the equilibration run, the interaction between PEG-DA and the terminal S of each chain is changed to Morse potential with the appropriate value of D, β and b to simulate the binding of PEG-DA to reactive group and an NPT simulation is performed for 2 μs. After the NPT, if the distance between the reactive group and a PEG-DA unit is smaller than 0.165 nm, the PEG-DA is considered bound to the reactive group. This threshold is selected by finding the distance distribution between PEG-DA and A, as in [108-109]. The Morse potential for each pair of bound PEG-DA-A is replaced by a permanent harmonic bond potential. Finally, within each precursor chain (now bound in a network) we perform an NPT run for 10 μs to simulate the new interaction of groups and then perform an NVT run for 400 ns to relax the system. Each of the subsequent simulations of Models I and II originates with this fixed permanent network.

2.3.3 Metal crosslinking

In the experiments in [8], the total metal ion molar concentration is fixed at 0.5 M, so we also fixed the total number of Fe ions in our simulations. After the hydrogel is formed, we simulate the formation of metal crosslinks by adding the total number of 2500 of Fe^{3+} and Fe^{2+} crosslinkers to the system while fixing the Fe^{3+}/A fraction to be a number between 0 and 0.5. This affects also the Fe^{3+}/ Fe^{2+} fraction because the total number of Fe^{3+} and Fe^{2+} ions remains 2500. Similarly to the network formation process, we first place crosslinkers in the simulation cell, then relax the system using the NVT ensemble for 10 ns. As in the NVT process of network simulation, the interactions between the reactive groups and crosslinkers during this phase are governed by just the WCA potential. Then, similarly to the network formation, the interaction between A and Fe^{3+} is changed

to Morse potential with the appropriate values of D, β and b as discussed in the previous section, and the formation of the metal crosslinks is simulated by an NPT process for 20 ns.

2.3.4 Network deformation

To study elastic properties of the hydrogel, we deform the simulation cell along the z-axis while keeping its volume fixed due to the incompressible nature of the hydrogel during the deformation. The network deformation is performed with and without metal crosslinks in order to understand how the elastic properties change due to the metal crosslinks.

The constant volume uniaxial deformation is realized by stepwise increasing the dimension of the simulation cell along the z-axis at a fixed deformation rate of 0.002 nm/ps while concurrently decreasing the dimension of the cell in the x- and y-directions appropriately at each time step, so that after 500 ps the volume of the system remains the same but the dimension of the hydrogel along the z-axis is 0.5 nm longer. After each 500 ps deformation, an NVT run is performed for 5 ns to relax the polymer network with the new cell shape. The average values of the components of the stress tensor $\sigma = -\mathbb{P}$ (see Equation (2.14)) are obtained from the second half of the NVT simulation, when the system is in an equilibrium state. In our project, we are interested in the uniaxial stress σ_{zz} which we use to compute the Young's modulus of the hydrogel. In what follows, by stress we mean the component σ_{zz}. For deformation and relaxation processes we do not change the potential types between the groups. We repeat the deformation-relaxation process four times in order to calculate the modulus of the hydrogel. For each time, the strain $\varepsilon = \Delta L/L_0$, with ΔL and L_0 are the change in z-dimension and the original z-dimension of the simulation cell, respectively.

The three stages of simulation of the network are illustrated in Figure 2.2 together with schematic diagrams of the system and examples of actual configurations of the network.

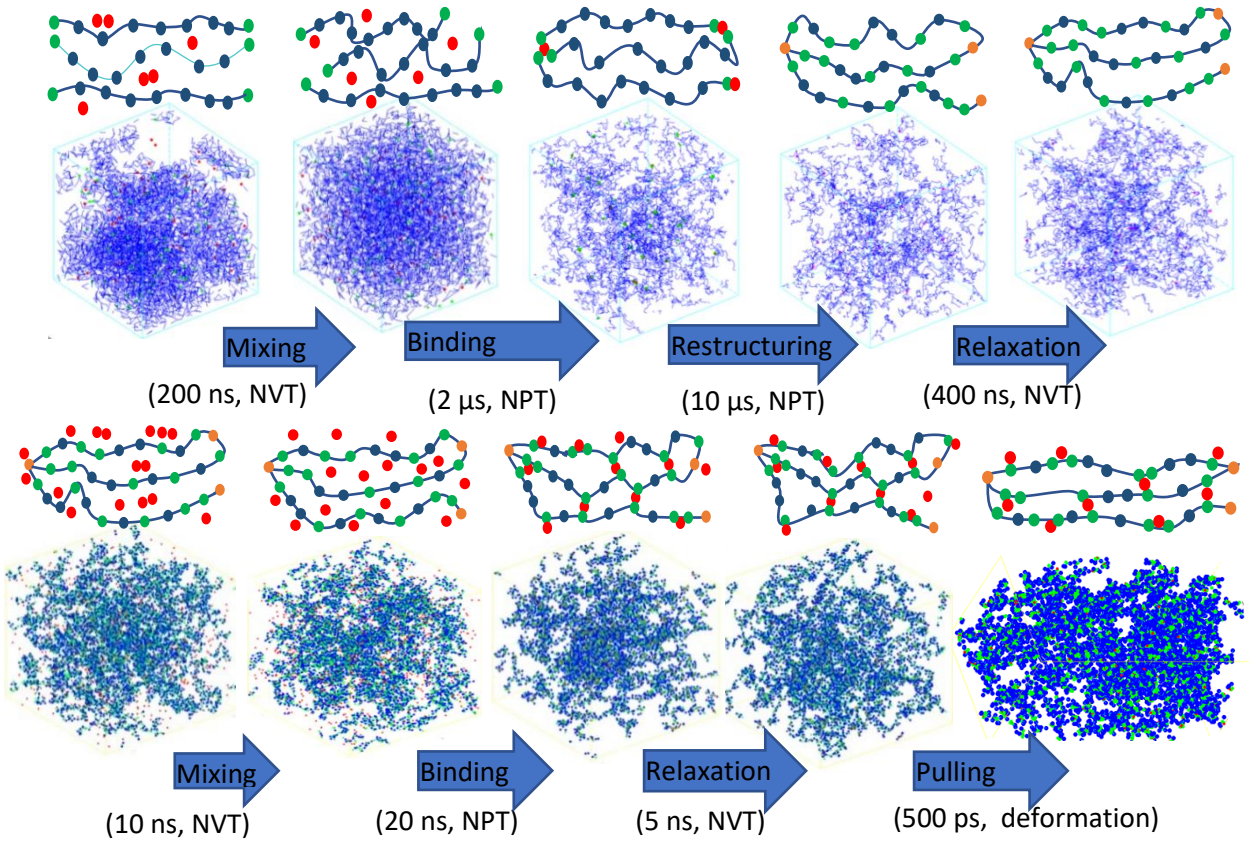

Figure 2.2. Diagram depicting the order of simulation steps, schematic representation of the formation of the permanent network (top row) and an example of network configuration that includes Fe^{3+} (bottom row). In the schematic representation crosslinker units are shown in red and reactive groups in green.

3.0 COVALENT NETWORK

3.1 NETWORK FORMATION

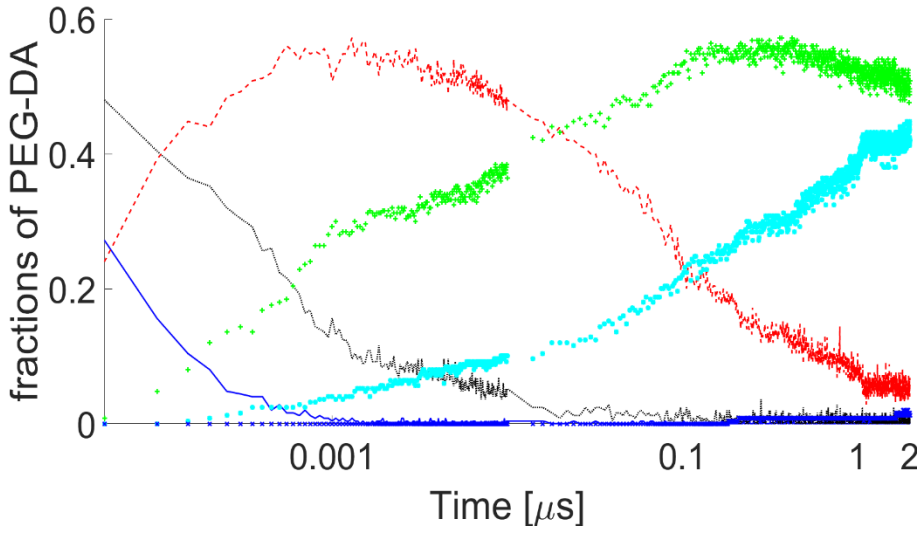

Figure 3.1. Time evolution of fractions of PEG-DA that are bound to different numbers of reactive groups: zero (solid blue curve), one (black), two (red), three (green), four (cyan) and five (blue markers).

The first step in our hydrogel simulation is the formation of a covalently bonded polymer network. To this network we later add metal crosslinks in Model I and Model II. The formation of the polymer network from the precursor chains can be illustrated by characteristics such as the fractions of PEG-DA with different coordination numbers. When PEG-DA are added to the simulation cell, initially they are not bound to any reactive groups, but soon all PEG-DAs are bound to at least one A group, as shown in Figure 3.1. The fraction of PEG-DAs that are bound to just one reactive group rapidly increases, reaches its maximum and then decreases to about 1%.

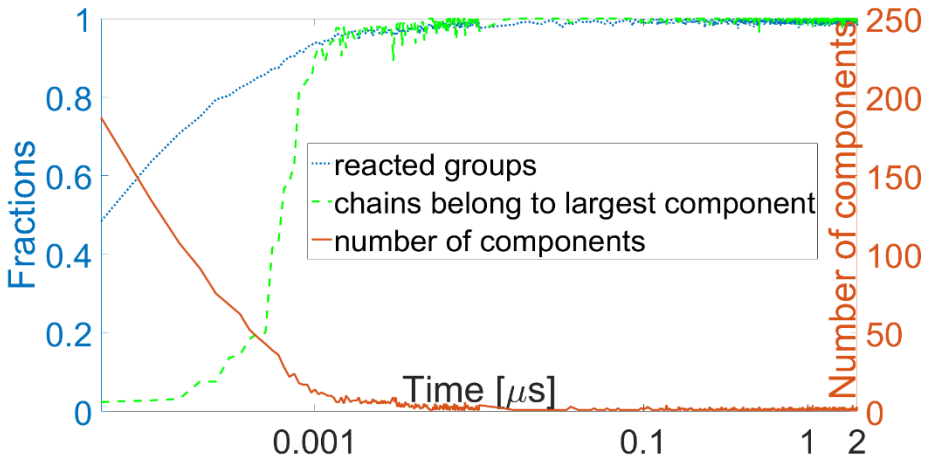

Figure 3.2. Time evolution of the fractions of reacted groups (dotted blue, left y-axis), the number of chains belonging to the largest component (dashed green, left y-axis), and the evolution of the number of components (solid orange, right y-axis).

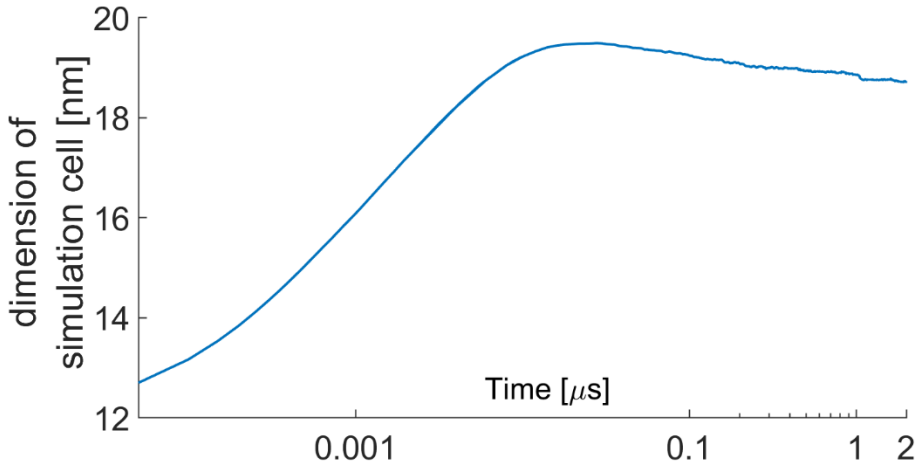

Figure 3.3. Time evolution of the dimension of each side of the simulation cell during the formation of the polymer network.

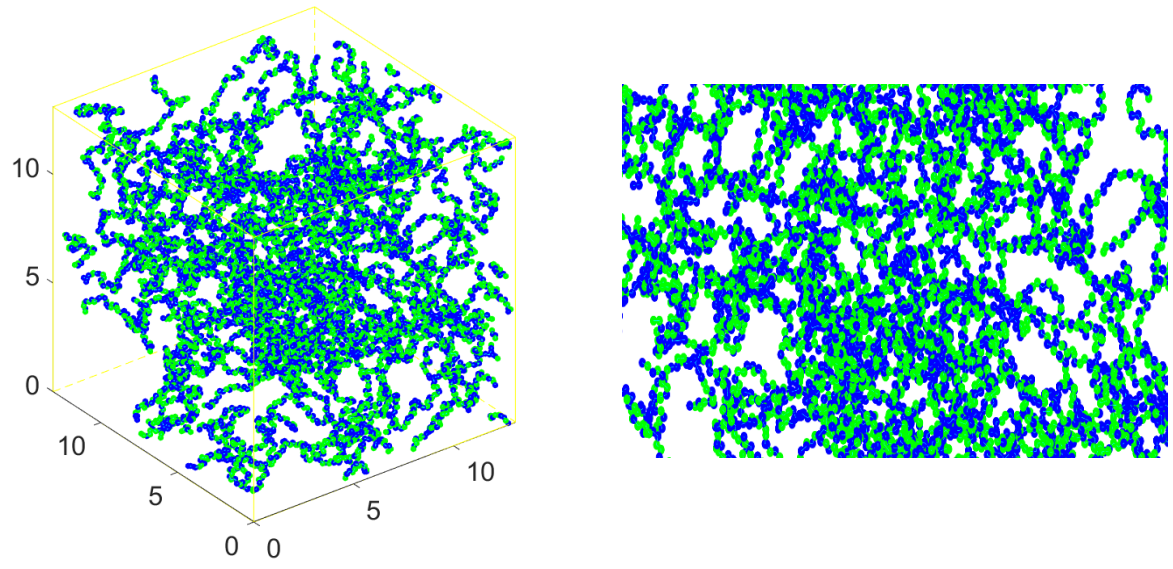

(a) (b)

Figure 3.4. The hydrogel at the end of the network formation: (a) One periodic cell of the network (b) Enlarged view of a part of the network.

The fraction of PEG-DA bound to exactly two groups reaches its maximum after 1 ns, then decreases gradually and remains approximately 0.1. PEG-DAs bound to five reactive groups appear after about 100 ns, after which their fraction increases and finally stabilizes at 2%. At the end of our simulation, the largest fractions are taken up by PEG-DA bound to three or four reactive groups, which make up about 52% and 34%, respectively. A reactive group that binds to a PEG-DA crosslinker is called a reacted group. We analyze the number of reacted groups, the number of chains belonging to the largest component and the number of components in the network. Early in the simulation, the number of reacted groups is larger than the number of chains belonging to the largest component but soon they become nearly equal and both fractions approach 1, as shown in Figure 3.2. This is reasonable because components formed via reacted groups need time to form larger components, and eventually only one component remains, as the solid curve shows. From the curves, we see that at the time when 50% reactive groups have undergone reaction, there are still more than 100 components.

We illustrate the change of dimension of the simulation cell in Figure 3.3. It rapidly increases from the initial value of 10 nm to maximum dimension of 19.48 nm then slowly goes to its equilibrium value of 18.71 nm. That could be explained by the steric repulsion and the binding process between the groups in the system during the simulation.

Although the coordination numbers of PEG-DA crosslinkers appear to be still changing at the end of the simulation (Figure 3.1), we consider the configuration at 2 μs to have satisfactory topological properties, i.e., there is only one component in the network and the maximum number of reactive groups bound to a PEG-DA group is four. We retained this network as the permanent reference polymer network on which all of the remaining simulations are performed. As mentioned in Section 2.3, the Morse potential for each pair of bound PEG-DA-A is replaced by a harmonic bond potential to make all newly formed bonds permanent. That is the restructuring step in the schematic diagrams in Figure 2.2.

After relaxing the system, we have a hydrogel network with 5000 A groups and 5000 S groups and the dimension of 13.4 nm. In the hydrogel, each chain containing an A group bound to a PEG-DA represents for one chain arm bound to that PEG-DA. The above results show that the maximum number of arms bound to a PEG-DA is 4, as mentioned in Section 1.3.2. We illustrate the hydrogel in Figure 3.4.

3.2 NETWORK DEFORMATION

We now analyze the elastic properties of the hydrogel. We deform the hydrogel as described in Section 2.3.4 and plot the stress vs strain curve in Figure 3.5. The curve shows a linear dependence of stress on strain from 0 to 0.2, and nonlinear dependence at higher strains reflecting a stiffening of the hydrogel. The stiffening of hydrogel is in agreement with experimental observations [8, 49], polymer network theory and simulation results in [108-109]. The reason for this stiffening is that the initial elasticity is due to entropic forces resisting straightening of the chains while the stiffer

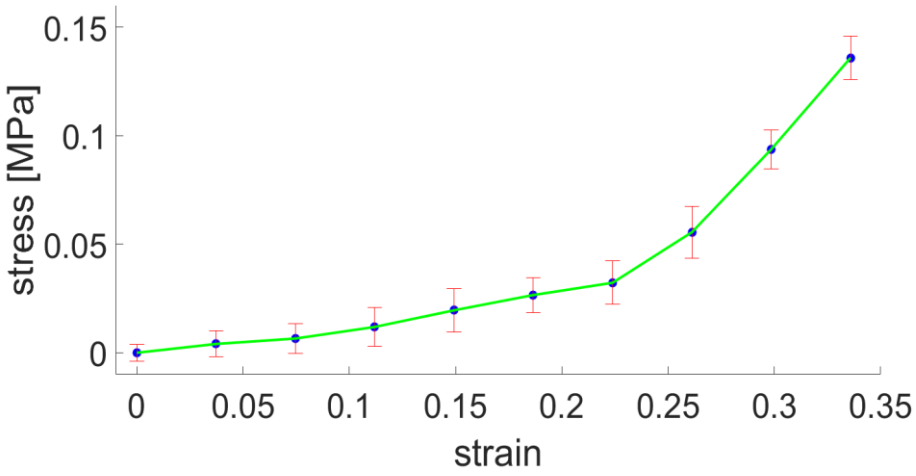

Figure 3.5. Stress vs strain curve for the original hydrogel

part is due to chain potentials, specifically the bond angle potential. The slope of the linear portion of the curve defines the elastic modulus of the hydrogel and it is 0.16 MPa. To obtain the averaged curve shown in Figure 3.5, we deformed the hydrogel nine times. However, to compute the elastic modulus, we need only 5 initial points in the curve, which form its linear portion. Later, in Chapter 4 and Chapter 6, for the hydrogel with added Fe^{2+} and Fe^{3+}, we also deform only four times to calculate the elastic modulus.

4.0 MODEL I

The next step of our hydrogel simulation is the addition of Fe^{3+} and Fe^{2+} cations and the formation

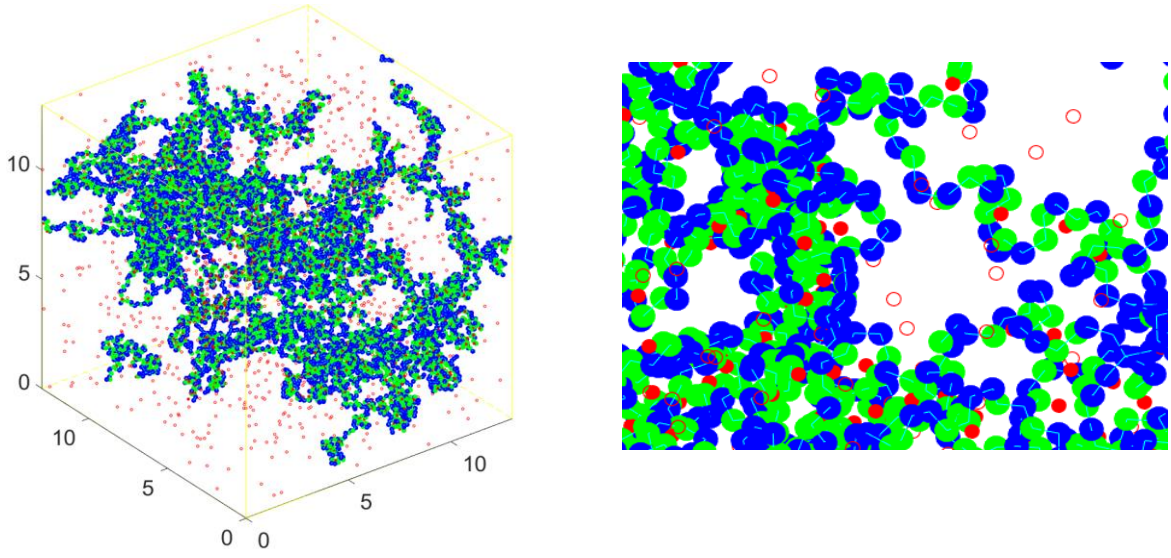

(a) (b)

Figure 4.1. The hydrogel with 1500 $Fe^{3+}$and 1000 Fe^{2+} at the end of the metal crosslinking simulation. (a) The whole hydrogel (b) Enlarged view of a part of the network.

of additional crosslinks in the polymer network. In this model, although both cations are added to the system, only the Fe^{3+} ions can form temporary bonds with the A groups.

As mentioned in Chapter 2, a crosslink is considered to be formed between an A group and a Fe^{3+} atom when the distance between the point masses representing them is less than $b + \ln(2)/\beta \approx 0.16621$ nm, the value at which the attractive force formed by the Morse potential attains its maximum. Figure 4.1 illustrates the hydrogel after the metal crosslinking step with 1500

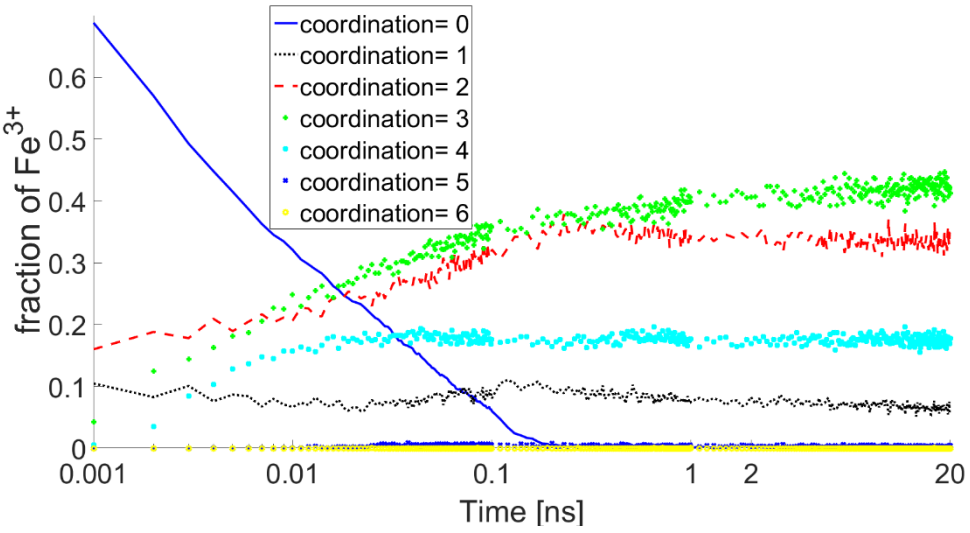

Figure 4.2. Time evolution of fractions of 1500 Fe^{3+} that are bound to different numbers of reactive groups: zero (solid blue curve), one (dotted black), two (dashed red), three (green pluses), four (cyan stars, five (blue crosses) and six (yellow circles)

Fe^{3+} and 1000 Fe^{2+}. The atoms surrounding the polymer groups in Figure 4.1a are Fe^{2+}, which cannot bind to A groups. In Figure 4.1b, they are represented by the hollow red circles. In contrast, Fe^{3+} ions (solid red circles) can form bonds with A groups (green circles). The blue circles represent the S groups which cannot bind to Fe^{3+}.

We investigate internal properties of the hydrogel by analyzing the time evolution of several characteristic quantities in a simulation. In Sections 4.1- 4.3 we consider the simulation with 1500 Fe^{3+} and 1000 Fe^{2+}, the Fe^{3+}/A fraction 1500/5000=0.3 and the Fe^{3+}/ Fe^{2+} fraction 1500/1000=1.5. In our simulations, we change some Fe^{3+} ions into Fe^{2+} ions in order to change the Fe^{3+}/A fraction. Throughout this chapter we also investigate how some characteristic quantities of the simulations change when the Fe^{3+}/A fraction is varied while the total Fe is kept fixed at 2500 groups. That helps us compare the effects of Fe^{3+} with those of Fe^{2+} on the hydrogel.

4.1 COORDINATION PROPERTIES

To monitor the dynamics of additional crosslink formation, we use the same approach as in the previous section and monitor the proportions of Fe^{3+} with different coordination numbers during the 20 ns NPT binding simulation. Figure 4.2 shows the time evolution of fractions of 1500 Fe^{3+} that are bound to different numbers of the A groups. In the beginning of the NPT simulation, all Fe^{3+} ions do not bind to any A group, but after 0.001 ns, the fraction of free Fe^{3+} (the Fe^{3+} ions which is not bound to any A group) decreases to 0.7. After 0.1 ns, most of Fe^{3+} ions bind to at least one A group. After 1 ns, the fractions of Fe^{3+} with coordination of one, two, three, four and five A groups increase to 8%, 33%, 41% and 17%, respectively. The total fraction of Fe^{3+} with coordination zero, five or six is 1%.

Figure 4.3a shows the distribution of the coordination number for 1500 Fe^{3+} at the last time frame, i.e., after 20 ns of the binding simulation. The coordination numbers vary from 1 to 5 with the average of 2.69. The coordination of Fe^{3+} for all proportions of Fe^{3+}/A varies from 0 to 6, and the average coordination at equilibrium state changes from 3.7 to 1.8, as shown in Figure 4.3b. For the higher Fe^{3+}/A fraction, the average coordination is smaller. This is not surprising because as the fraction increases, the average of number of A groups available for one Fe^{3+} becomes smaller, and in all simulations, there are very few free Fe^{3+} ions and complex components (see Section 4.3). At Fe^{3+}/A fraction of 0.5, two A groups can be bound to each Fe^{3+} ion with no groups or ions left free. As in Figure 4.4, the fraction of free Fe^{3+} (relative to the total number of Fe^{3+} ions in each simulation) varies between 0% and 1% in most simulations, and increases to 2.5% when the Fe^{3+}/A fraction of 0.5. The coordination numbers reflect the properties we discussed in Section 1.3 except there are some Fe^{3+} ions with coordination number of six.

4.2 DYNAMICS OF METAL CROSSLINKS

We divide 20 ns duration of the binding simulation to 200 time intervals, each of 100 ps duration.

For each 100 ps time interval, we calculate the following four quantities: the total number of crosslinks and the numbers of the retained, broken and newly formed crosslinks after each 100 ps. We illustrate the time evolution of these four numbers for the simulation with 1500 Fe^{3+} in Figure 4.5. From the graphs, we see that all four numbers quickly approach their equilibrium values after 0.2 ns. The number of broken and the number of newly formed crosslinks are both around 550,

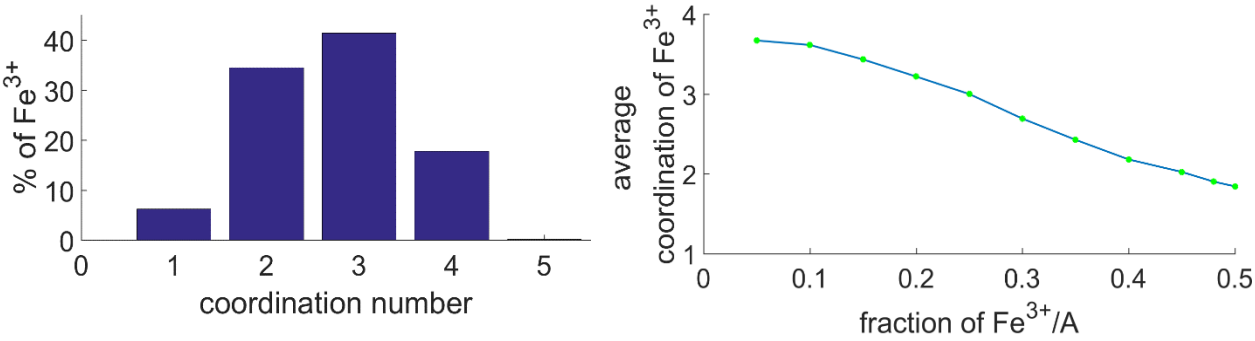

(a) (b)

Figure 4.3. The coordination number of Fe^{3+} ions. (a) Distribution of coordination number for 1500 Fe^{3+} at the end of the binding process. (b) Average coordination number of Fe^{3+} at the end of the binding process for different Fe^{3+}/A ratios.

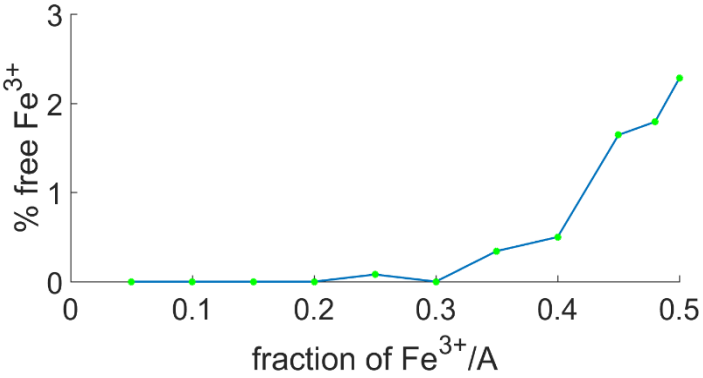

Figure 4.4. The percentage of free Fe^{3+} at the end of the binding process for different Fe^{3+}/A ratios.

which is approximately 13.5% of the total number of crosslinks (around 4100). So although the total number of metal crosslinks remains the same in an equilibrium state, the processes of

retaining, breaking and newly forming of crosslinks are dynamic.

To better understand these processes, we divide the first and the last 100 ps time intervals into

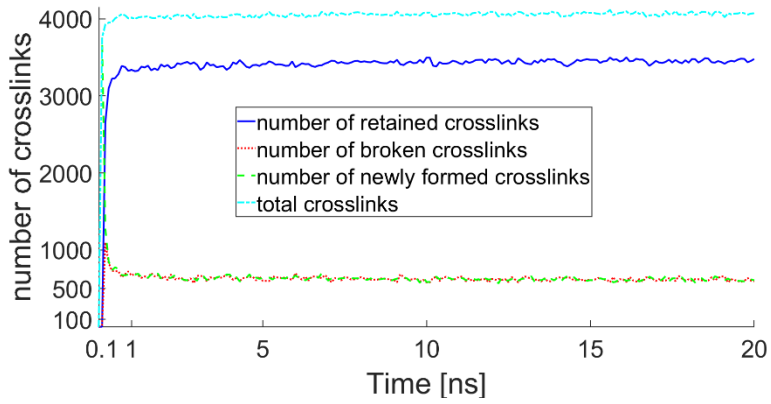

Figure 4.5. Time evolution of number of crosslinks of different types during each 100 ps subinterval for simulation of 1500 Fe^{3+}: retained (solid blue), broken (dotted red), newly formed (dashed green), and total (dash dotted cyan) crosslinks.

100 subintervals of duration 1 ps each, and find the statistics shown in Figure 4.6. We see that during the first 100 ps, the four numbers increase to their equilibrium values. And during the last 100 ps the four numbers are not very different from the ones in Figure 4.5. During each 1 ps subinterval of the period of 100 ps, there are about 500 broken and newly formed crosslinks, but the total number of crosslinks at the end of the period is about 4000. It means that during a 100 ps time period many crosslinks get broken and then form again, and vice versa. In Chapter 6, we will consider Model II, where Fe^{2+} can also form crosslinks, and compare the dynamics of crosslinks formed by Fe^{3+} and Fe^{2+}.

4.3 COMPLEX COMPONENTS

As mentioned in Chapter 1, a complex component is formed when an A group bound to two or more crosslinkers. Experiments show that there are complex components in the hydrogel [9]. The

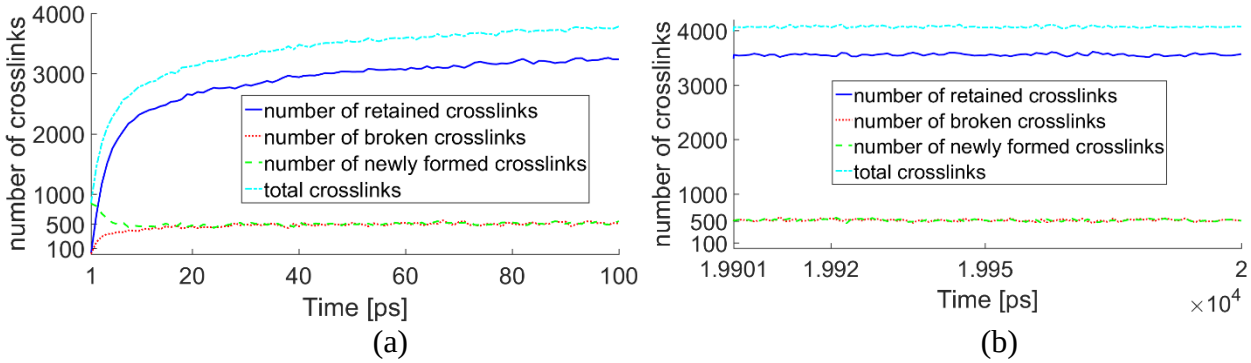

Figure 4.6. Time evolution of number of crosslinks of different types in each 1 ps for simulation of 1500 Fe^{3+}: retained (blue solid), broken (dotted red), newly formed (green dash), and total (dash dotted cyan) crosslinks. (a) first 100 ps of the simulation (b) last 100 ps of the simulation

corresponding simulation results are shown in Figure 4.7. As shown in Figure 4.7a, for the simulations reported in this section, only about 1% of the A groups are bound to two or more Fe^{3+}. Thus in our simulation there are very few complex components. In Figure 4.7b, we see that although the average number of Fe^{3+} bound to a single A group increases as the Fe^{3+}/A fraction grows, this number is less than 1.02, so the number of complex components remains small in all simulations. This agrees with the fact that there are complex components in the hydrogel in the experiments [8-9].

4.4 COMPACTION OF FE-HYDROGEL

We know that when we add material to an equilibrium system, the steric repulsion will make the volume larger and the binding process will make the system smaller. When there are only Fe^{2+} added to the hydrogel (i.e., the system includes zero Fe^{3+} and 2500 Fe^{2+} in addition of the permanent network), the addition steric repulsion makes the length of each side of the simulation cell increase from 13.4 nm to 23.23 nm. This behavior mimics the swelling of the hydrogel with water. The cell size decreases as we increase the Fe^{3+}/A ratio. This is due to the binding process between Fe^{3+} and A groups. As mentioned in Section 2.3.1.2, we can understand the change of the

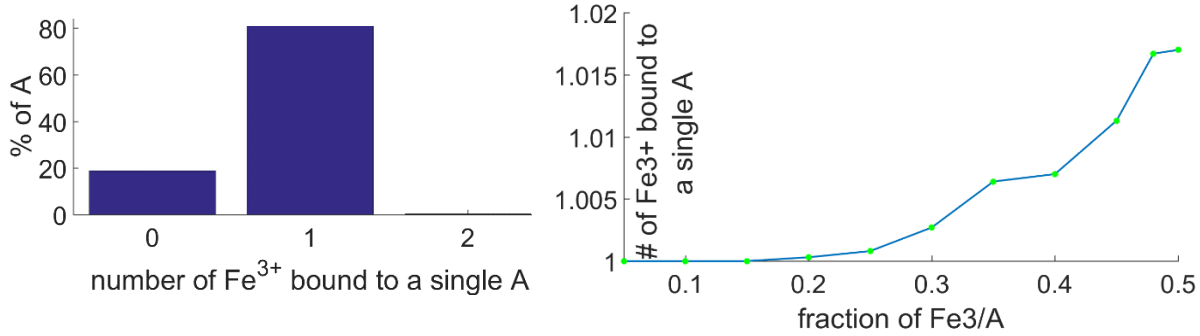

Figure 4.7. Some statistical results for the number of Fe^{3+} bound to a single A group: (a) the distribution of the number of Fe^{3+} bound to a single A group (1500 Fe^{3+} at the end of binding process). (b) the average number of Fe^{3+} bound to a single A group at the end of binding process for different Fe^{3+}/A ratios.

size of the hydrogel by analyzing the change of size of the simulation cell. As a result, the size of the hydrogel is a monotone decreasing function of the Fe^{3+}/A fraction, as shown in Figure 4.8.

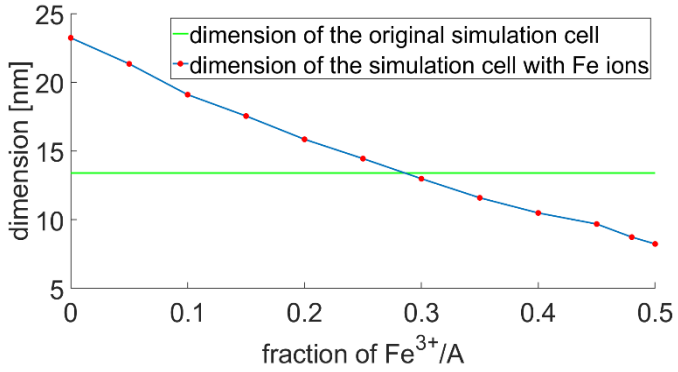

Figure 4.8. Dimension of the simulation cell as the function of Fe^{3+}/A fraction

We see in Figure 4.9a that the size of the simulation cell, and hence the volume of the cell, decreases during the binding process with 1500 Fe^{3+} added. The contraction of the hydrogel is

associated with the decrease of the average distances between the groups in it. We define the average distances as follows:

$d_s = \overline{d_{PQ}}$, for all groups P and Q in a single chain, over all chains

$d_d = \overline{d_{PQ}}$, for all groups P and Q in two different chains, over all chains

$d_a = \overline{d_{PQ}}$, for all groups P and Q in the hydrogel, over all chains

The formula of d_s, d_d and d_a are

$$d_s = \sum_{i=1}^{250} \sum_{\substack{P,Q \in chain\ i \\ P \neq Q}} d_{PQ} \cdot \frac{1}{number\ of\ pairs\ (P,Q)}$$

$$d_d = \sum_{\substack{i,j=1 \\ i \neq j}}^{250} \sum_{P \in chain\ i}^{Q \in chain\ j} d_{PQ} \cdot \frac{1}{number\ of\ pairs\ (P,Q)}$$

$$d_a = \sum_{i,j=1}^{250} \sum_{\substack{P \in chain\ i \\ Q \in chain\ j \\ P \neq Q}} d_{PQ} \cdot \frac{1}{number\ of\ pairs\ (P,Q)}$$

As shown in Figure 4.9b, the values of d_s, d_d and d_a are decreasing as the Fe^{3+}/A fraction grows. We now analyze the reasons for this decrease.

The decrease of d_s is associated mainly with the formation of loops. We see in Figure 4.10b that there are many loops in the hydrogel. The total number of loops increases as the Fe^{3+}/A fraction grows from 0 to 0.4, and decreases for larger fractions. The number of loops may be larger than the number of Fe^{3+} ions because one ion can form more than one loop in a chain. To better understand the structure of the hydrogel, we investigate the number of short loops and the number of long loops. One can see that the number of long loops is almost constant while the number of short loops monotonically increases together with the total number of loops as the Fe^{3+}/A fraction

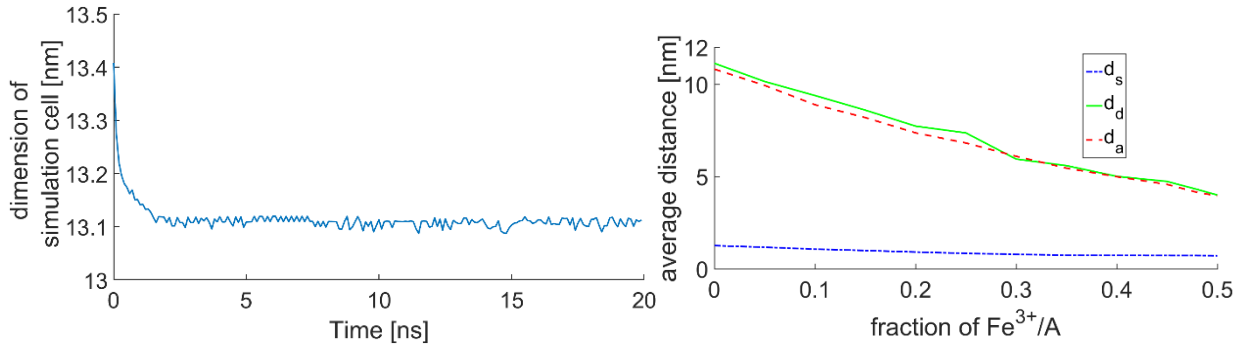

(a) (b)

Figure 4.9. The dimension of the simulation cell and the average distance between the groups. (a) Time evolution of the dimension of the simulation cell during the simulation of 1500 Fe^{3+} (b) Average distance between the groups of the polymer network in the hydrogel with different density of Fe^{3+}/A: groups in a single chain (dash dotted blue), groups in two different chains (dotted red) and groups in the entire polymer network (solid green)

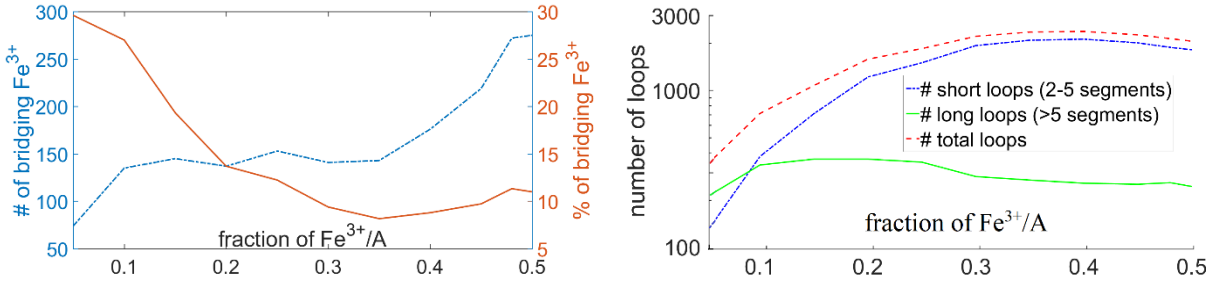

(a) (b)

Figure 4.10. The number of bridging Fe^{3+} and the number of loops. (a) The number of bridging Fe^{3+}(dash dotted blue, left axis) and the percentage of bridging Fe^{3+} (over the total Fe^{3+} for each simulation) as Fe^{3+}/A fraction is varied. (b) The number of loops as the function of Fe^{3+}/A fraction: short loops (dash dotted blue), large loops (solid green), all loops (dashed red)

grows. We conclude that adding more Fe^{3+} does not contribute to formation of long loops but results instead in the creation of more short loops. This in turn decreases the average distance

between groups in a single chain.

The bridging Fe^{3+} ions, i.e., the ions that are bound to two or more different chains, contribute to making the distances between groups in different chains shorter. As shown in Figure 4.10a, the percentage of bridging Fe^{3+} varies from 10% to 30%, and the number of bridging Fe^{3+} mostly increases with the Fe^{3+}/A fraction. While the number of bridging Fe^{3+} remains relatively small (less than 300), in combination with the loops, they make the average distance between groups in different chains d_d and the average distance between two groups d_a shorter, as shown in Figure 4.9b.

4.5 ELASTIC MODULUS

In Figure 4.11, we show how the elastic modulus of the hydrogel varies with Fe^{3+}/A and Fe^{3+}/Fe^{2+} fractions under the uniaxial deformation. The modulus in our simulations increases significantly

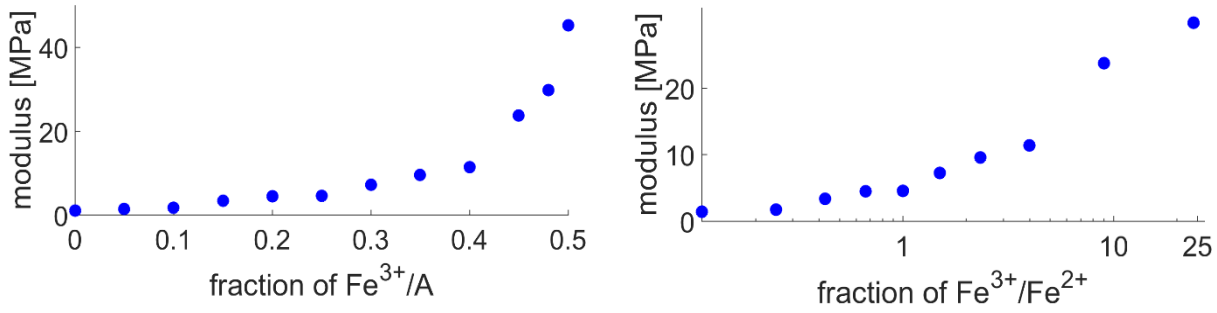

(a) (b)

Figure 4.11. Elastic modulus of the hydrogel as (a) Fe^{3+}/A and (b) Fe^{3+}/Fe^{2+} fractions are varied.

as the Fe^{3+}/A and Fe^{3+}/Fe^{2+} fractions increase, in qualitative agreement with experimental results shown in Figure 1.2.

To explain the increase in the elastic modulus as the density of Fe^{3+}/A increases, we consider separately the effects of bridging Fe^{3+} and all bound Fe^{3+}, i.e., the Fe^{3+} ions that are bound at least one chain (including the bridging irons).

4.5.1 Effects of bound Fe^{3+} on elastic modulus of hydrogel

In our network, every chain contains 39 units made from 40 groups that are numbered from position 1 to 40. Due to the large number of units in every chain, each chain can assume many different shapes when the network is stretched. Each bound Fe^{3+} is bound to the A groups at some positions in one or more chains. As shown in Figure 4.12a, there are many Fe^{3+} ions at each A position in a chain. This amounts to the Fe^{3+} ions separating a chain into a number of smaller segments at the positions they are bound to, therefore shortening the effective average length of a chain.

Calculating the average number of units in the effective chains (segments of the original chains) at the equilibrium state in the simulations with different Fe^{3+}/A fractions, we obtain the graph shown in Figure 4.12b. One can see that the average number of units in an effective chain rapidly decreases from 39 to 3 when the Fe^{3+}/A fraction varies from zero to 0.2 and decreases further to 2.05 when the Fe^{3+}/A fraction reaches 0.5. Thus, the number of units in effective chains is very small compared to the original chains. Shortening the length of effective chains makes the hydrogel stiffer.

4.5.2 Effects of bridging Fe^{3+} on elastic modulus of hydrogel

Clearly, bridging Fe^{3+} ions are bound Fe^{3+}, so they shorten the effective lengths of the chains as described above. However, they also prevent a chain from slipping past the other chains. This makes the hydrogel stiffer. In this section we discuss two other characteristic quantities related to the bridging Fe^{3+} that make the hydrogel stiffer. These are the percentage of crosslinked chains and the number of chains bound to a single chain.

As shown in Figure 4.13a, the fraction of non-crosslinked-chains is about 43%. It is close to

the fraction of chains bound to a single chain. There are about 10% of chains bound to two chains. There are very few chains bound to three chains and no chains bound to four or more chains. In this simulation the Fe^{3+}/A fraction with 1500 Fe^{3+} is 0.3 and corresponds to the plateau in the two graphs shown in Figure 4.13b. As shown in Figure 4.11a, the elastic modulus increases significantly when the Fe^{3+}/A fraction exceeds 0.4.

To compare effects of bridging Fe^{3+} with the effects of bound Fe^{3+} discussed above, let us consider the Fe^{3+}/A fraction in the range of [0.4, 0.5]. In this range, as shown in Figure 4.11a, the modulus increases from 10 MPa to 44 MPa. To better understand the topology of Fe-hydrogel network, we consider the crosslinked-chains, i.e., the chains bound to at least one another chain. Figure 4.13b shows that both the percentage of crosslinked-chains and the number of chains bound to a chain increase significantly in this fraction range. On the other hand, according to Figure 4.12b, the number of units in an effective chain is nearly constant when the Fe^{3+}/A fraction is in the range of [0.4, 0.5]. So we can conclude that the significant increase of the elastic modulus in this range is due to the bridging Fe^{3+}.

Similarly to the binding step (See Section 4.2), during the elastic network deformation, many crosslinks are newly formed or get broken and then form again, resulting in newly formed or untenable bridging Fe^{3+} ions. However, the number of bridging Fe^{3+} ions are almost unchanged and similar to the binding step (See Figure 4.10a).

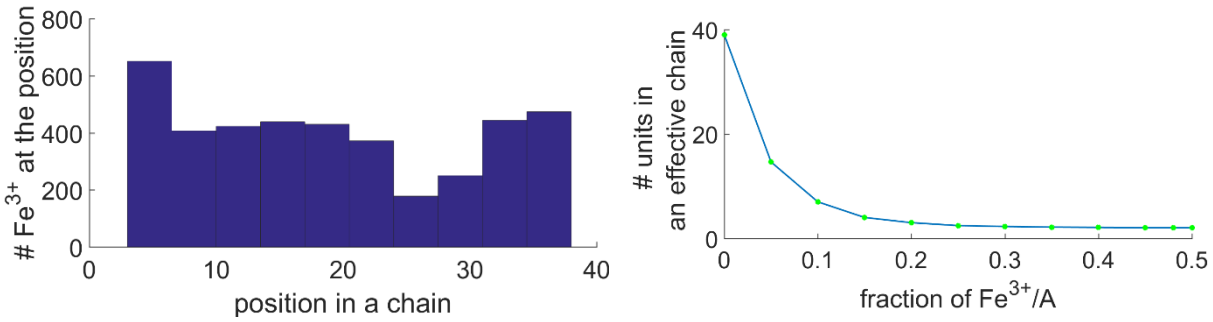

(a) (b)

Figure 4.12. The shortening of the effective chains by Fe^{3+}. (a) Histogram of Fe^{3+} position in a chain at the end of the binding process in the simulation of 1500 Fe^{3+} (b) Average number of units in an effective chain.

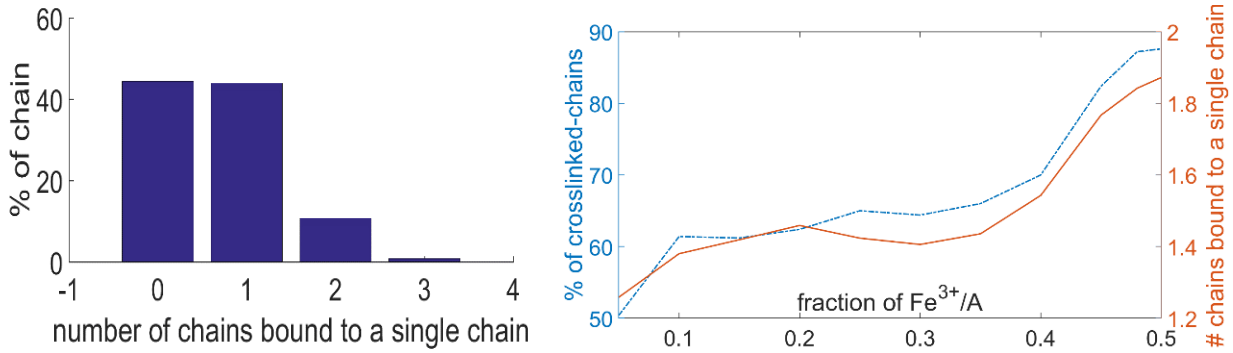

(a) (b)

Figure 4.13. The number of chains bound to a single chain. (a) Histogram of percentage of chains in the hydrogel bound to number of different chains at the end of binding process in the simulation of 1500 Fe^{3+} (b) Percentage of crosslinked-chain (dash dotted blue, left y-axis), and average number of chains bound to a single chain (solid orange, right y-axis)

5.0 MODEL II CALIBRATION

As we saw in Section 4.4, the size of the simulation cell decreases when the number of Fe^{3+} increases. As a result, the size of hydrogel is a monotone decreasing function of Fe^{3+}/A fraction as shown in Figure 4.8. However, the size of the simulation cell of the original permanent network (without Fe^{3+} and Fe^{2+}) is 13.40 nm, and the size turns to be larger for hydrogel with Fe^{3+}/A ratio of 0.25 or smaller. That means the Model I, in which Fe^{2+} ions do not bind to A groups, does not reflect the compaction of hydrogel when the Fe^{2+}/A ratio is 0.25 or higher. As we will show below in Chapter 6, the Model II, in which Fe^{2+} bind weakly to A groups, does not suffer from this deficiency: when Fe^{2+} are allowed to form bonds, the hydrogel reduces in volume when Fe^{2+} is added and exhibits even more compaction with added Fe^{3+}.

As discussed in Chapter 1, our models define a type of crosslinker by the choice of interaction potentials between crosslinkers and groups in the hydrogel or between crosslinkers themselves. If some of these potentials change, we have a different type of crosslinker. Crosslinkers of different types yield different characteristic quantities of the hydrogel.

In Model I, we treat Fe^{2+} as neutral atoms that only affect how hydrogel swells up, i.e., increases in volume. In this chapter, we construct a model of a hydrogel where both Fe^{3+} and Fe^{2+} can bind to A groups with different affinities and hence we have two types of crosslinkers. The binding mechanism of Fe^{2+} is assumed to be via the same potentials as Fe^{3+} but with different parameters, i.e., we change the parameters of the Morse potential between the crosslinkers and the A groups or the WCA potentials between the crosslinkers and the groups in the system or between the crosslinkers themselves. In this chapter, we use the relations obtained from the computer simulations to select suitable values of parameters for Fe^{3+} and Fe^{2+}, so that our model qualitatively

reflects the experimental findings. These parameters are then used to obtain the results for Model II described in Chapter 6.

As we saw in Chapter 2, the Morse and WCA potentials we use reflect both the steric repulsion and electrostatic forces between the groups. In this chapter, we seek to include two types of crosslinkers, so we focus on interaction potentials which reflect primarily for electrostatic forces. These are the Morse potential governing the interactions between the crosslinkers and the A groups, and the WCA potential for the interactions between the crosslinkers themselves.

In order to separate the effects of different types of crosslinkers, we will run the simulations with only one type of crosslinker in the system for each simulation. The number of crosslinkers for each simulation is 2500, as in Model I.

We aim to use simulation results to introduce two types of crosslinkers for Fe^{3+} and Fe^{2+} so that (with same amount of Fe^{3+} and Fe^{2+}) the model reflects the following experimentally observed properties discussed in Section 1.3:

(i) Both Fe^{3+}-hydrogel and Fe^{2+}-hydrogel are stiffer than the original hydrogel but the modulus of Fe^{3+}-hydrogel is significantly larger compared to Fe^{2+}-hydrogel

(ii) Both Fe^{3+}-hydrogel and Fe^{2+}-hydrogel are smaller in size compared to the original hydrogel, but the Fe^{3+}-hydrogel are more compact.

(iii) The average coordination number of Fe^{3+} is in the range from 2 to 4, while the average coordination number of Fe^{2+} is very small compared to Fe^{3+}.

5.1 RELATIONS BETWEEN PARAMETERS OF MORSE POTENTIAL AND SOME CHARACTERISTIC QUANTITIES

Recall that the Morse potential has three parameters: b is the equilibrium distance between Fe and A, D controls the strength of the crosslink, and β controls the distance over which the potential is effective. By changing the values of D and β in simulations with the same number of crosslinkers,

we obtain the relations between the parameters and the characteristic quantities mentioned above.

In this section, we do not change the WCA potential between crosslinkers but run the simulations for different parameters of Morse potential. We consider four different values of D: 30, 45, 60, 90 (kJ mol^{-1}) and three different values of β: 12.5, 15, 20 (nm^{-1}). Other parameters of Model I (in the Table 2.1) are unchanged.

We performed simulations of the crosslink formation with different parameter values for the Morse potential to study the correlations of the parameters with the elastic modulus, the size of the simulation cell and the average coordination number of the crosslinkers.

5.1.1 Relations between Morse parameters and values of modulus and compaction

In Table 5.1 and 5.2, we present the values of the elastic modulus and the size of the simulation cell, respectively. In Table 5.1, the last value in each row is the correlation coefficient between values of the modulus in the row and corresponding values of β, and the last value in each column is the correlation coefficient between values of the modulus in the column and corresponding values of D. Similarly, in Table 5.2, we calculate the correlation coefficients for the dimension of simulation cell. Our goal in this section is to select the values of β, and D that best represent Fe^{3+} and Fe^{2+}.

Table 5.1. The elastic modulus (MPa) for different parameters of the Morse potential

D \ β	12.5	15	20	Correlation with β
90	255.95	45.27	1.14	-0.85
60	69.00	3.44	0.94	-0.78
45	22.76	2.20	0.73	-0.79
30	4.00	0.76	0.41	-0.81
Correlation with D	0.96	0.90	0.96	

Table 5.1 demonstrates that the elastic modulus increases as β decreases or D increases, resulting in the strong negative correlation of modulus with β and strong correlation of modulus

with D. In simulation, the modulus of the original hydrogel is 0.16 MPa. To reflect Properties (i) in Section 5.0, we can choose values of β=15 and D=30, or $\beta = 20$ and any $D \geq 30$ for Fe^{2+}. For these values, adding Fe^{2+} does not result in a significant increase of the elastic modulus. For Fe^{3+}, we can select values β=15 and D=90 (as in Model I), or $\beta = 12.5$ and D is in the range of [30, 90].

Table 5.2. The size of the simulation cell (nm) for different parameters of the Morse potential

D \ β	12.5	15	20	Correlation with β
90	7.84	8.24	11.96	0.97
60	8.15	8.81	12.43	0.98
45	8.27	9.52	12.67	1.00
30	8.55	11.68	13.66	0.95
Correlation with D	-0.99	-0.89	-0.92	

We now analyze the results included in Table 5.2. One can see that the size of simulation cell increases as β increase or D decreases. The size for the hydrogel without Fe is 13.4 nm. We consider the values of D and β which reflect Property (i). For D=30 and $\beta = 20$, the size is 13.66 nm. To have the hydrogel contract when Fe^{2+} is added as Property (ii), we thus should not choose these values of D and β for Fe^{2+}. Instead, we can select β=15 and D=30, or $\beta = 20$ and any $D \geq 45$ for Fe^{2+}. The crosslinkers corresponding to these values make the hydrogel contract.

5.1.2 Analyzing the coordination number

In this section, we analyze the coordination number of different types of crosslinkers. As we see in Table 5.3, we get a higher average coordination number as D or β increases. However, the coordination numbers for different types of crosslinkers are very similar and approximately equal to 2. Moreover, for most of the parameters we selected for Fe^{2+} and Fe^{3+} in Section 5.1.1, the average coordination number of Fe^{2+} is actually higher than the coordination number of Fe^{3+}. This

contradicts the property (iii) in Section 5.0. So we are not able to select suitable parameters for Fe^{3+} and Fe^{2+} within the class of crosslinkers that were considered in this section. We need to consider different types of crosslinkers.

Table 5.3. The average coordination number for different parameters of the Morse potential

D \ β	12.5	15	20	Correlation with β
90	1.84	1.88	1.92	0.98
60	1.76	1.80	1.90	1.00
45	1.69	1.79	1.87	0.97
30	1.65	1.72	1.76	0.96
Correlation with D	0.99	0.97	0.87	

Table 5.4. The percentage of free crosslinkers for different parameters of the Morse potential

D \ β	12.5	15	20	Correlation with β
90	4.12	2.28	0.28	0.93
60	4.80	1.80	0.12	0.95
45	5.60	1.96	0.56	0.98
30	7.40	3.80	3.40	1.00
Correlation with D	-0.79	-0.18	-0.88	

Table 5.5. The number of crosslinkers bound to a single A for different parameters of the Morse potential

D \ β	12.5	15	20	Correlation with β
90	1.06	1.02	1.00	1.00
60	1.02	1.00	1.00	1.00
45	1.01	1.00	1.00	1.00
30	1.01	1.00	1.00	1.00
Correlation with D	1.00	1.00	N/A	

5.2 FINDING APPROPRIATE TYPES OF CROSSLINKERS FOR FE^{3+} AND FE^{2+}

We will first use the analysis of coordination number presented in Section 4.1 to understand why the coordination number is almost unchanged for different types of crosslinkers. In our simulations, the fraction of crosslinker/A is 0.5 and as one can see in Table 5.4 and 5.5, there are very few free crosslinkers and complex components. So there are about two A groups for one crosslinker in average. To obtain larger coordination numbers, we need to increase the number of free crosslinkers or complex components. In this section, we increase the number of complex components for our new types of crosslinkers.

If we fix the equilibrium distance between a crosslinker and an A group, the number of crosslinkers bound to a single A will increase as the equilibrium distance between the crosslinkers decreases. In Section 2.1.2, we chose a larger value for equilibrium distance between crosslinkers than would be implied by their size in order to account for the electrostatic repulsion due to their positive charge and set it equal to $0.45\,nm$. Considering that the radius of Fe ions is very small compared to A and S groups because Fe consists a single atom, the values of equilibrium distance between crosslinkers of r_{FeFe}=0.35 nm still qualitatively reflects the physical properties of the groups, but this decreased distance will enable higher coordination numbers.

With this change in interactions between crosslinkers, we ran the simulations for the hydrogel with four different values of D: 20, 30, 40, 50 (kJ mol^{-1}) and three different values of β: 12.5, 15, 20 (nm^{-1}). We summarize the computational results below.

Table 5.6. The elastic modulus (MPa) for different parameters of the Morse potential (with r_{FeFe}=0.35 nm)

D \ β	12.5	15	20	Correlation with β
50	49.90	12.99	1.18	-0.89
40	32.28	6.19	0.73	-0.85
30	29.56	2.13	0.41	-0.79
20	4.38	1.15	0.40	-0.86
Correlation with D	0.94	0.99	0.97	

The results of the important characteristic quantities are presented in Table 5.6-5.10. We first need to check the relations similar to the ones considered in Section 5.1. From Table 5.6 and 5.7, one can see that there are still strong or negative strong correlations between the parameters and the values of the elastic modulus and hydrogel compaction. As β decreases or D increases, the modulus increases while the size of the simulation cell decreases.

Table 5.7. The size of the simulation cell (nm) for different parameters of the Morse potential (with r_{FeFe}=0.35 nm)

D \ β	12.5	15	20	Correlation with β
50	7.95	8.60	11.82	0.98
40	7.97	9.04	12.03	1.00
30	8.38	9.77	12.18	1.00
20	8.98	11.35	13.42	0.97
Correlation with D	-0.85	-0.90	-0.82	

We now consider Table 5.9 and 5.10. There are still very few free crosslinkers but the number of crosslinkers bound to a single A group is larger in comparison to Table 5.4 and Table 5.5. This allows more A groups can bind to one crosslinker, resulting in the higher average coordination numbers.

Similarly to Section 5.1, by combining the values of Tables 5.6, 5.7 and 5.8, we choose the values of β=20 and D=30 for Fe^{2+} and β=15 and D=50 for Fe^{3+} in Model II. For these parameters, when we add 2500 Fe^{2+} and 2500 Fe^{3+}, the sizes of the simulation cell are 12.2 nm and 8.6 nm, respectively.

The average coordination numbers of Fe^{2+} and Fe^{3+} are 1.82 and 2.1, respectively. Although the coordination numbers of Fe^{2+} are not sufficiently small, the other two main characteristic quantities, modulus and compaction, are qualitatively captured.

We simulate Fe^{3+} and Fe^{2+} for Model II with these parameter values and analyze the results in the next chapter.

Table 5.8. The average coordination number for different parameters of the Morse potential (with r_{FeFe}=0.35 nm)

D \ β	12.5	15	20	Correlation with β
50	2.10	2.10	2.15	1.00
40	1.96	1.99	2.01	0.89
30	1.78	1.81	1.82	0.97
20	1.61	1.68	1.70	0.97
Correlation with D	-0.95	-0.96	-0.95	

Table 5.9. The percentage of free crosslinkers for different parameters of the Morse potential (with r_{FeFe}=0.35 nm)

D \ β	12.5	15	20	Correlation with β
90	1.60	1.96	0.40	-0.93
60	2.28	2.84	0.96	-0.85
45	4.48	4.72	2.00	-0.90
30	9.48	8.04	7.16	-1.00
Correlation with D	0.99	1.00	1.00	

Table 5.10. The number of crosslinkers bound to a single A for different parameters of the Morse potential (with r_{FeFe}=0.35 nm)

D \ β	12.5	15	20	Correlation with β
90	1.39	1.26	1.14	-0.92
60	1.31	1.21	1.08	-0.98
45	1.22	1.12	1.05	-0.97
30	1.11	1.06	1.01	-1.00
Correlation with D	-0.96	-0.96	-0.84	

6.0 SIMULATION RESULTS FOR MODEL II

We now use the parameters selected in Section 5.2 and run computer simulations for the Model II of the hydrogel with added Fe^{3+} and Fe^{2+}. As in the Model I simulations, the total number of Fe^{3+} and Fe^{2+} is fixed at 2500 and the fraction of Fe^{3+}/A is varied between 0 and 0.5.

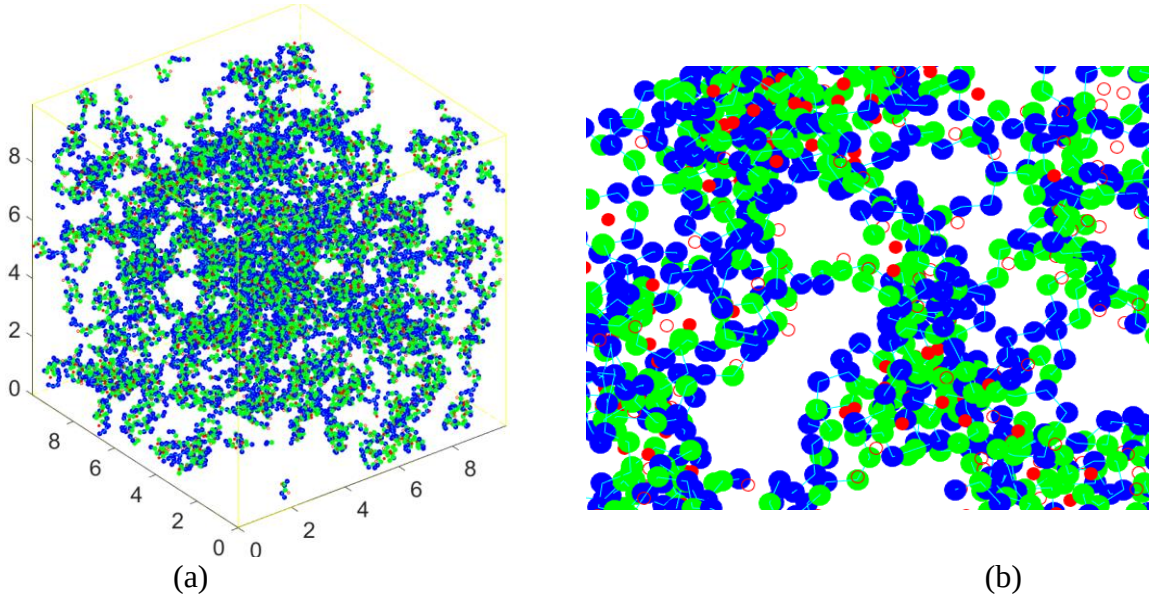

(a) (b)

Figure 6.1. The hydrogel with 1250 $Fe^{3+}$and 1250 Fe^{2+} at the end of the metal crosslinking simulation: (a) The whole hydrogel (b) Enlarged view of a part of the network.

In Figure 6.1, we show the hydrogel with 1250 Fe^{3+} and 1250 Fe^{2+} after the metal crosslinking step. In this model, both Fe^{3+} (solid circles) and Fe^{2+} (hollow circles) ions can form bonds with the A groups (green circles). However, from Figure 6.1b, comparing to Fe^{3+}, we expect that there is a smaller number of A groups bound to Fe^{2+} ions. We will check this in Section 6.1.

Similarly to Model I, we investigate the internal structure of the hydrogel and some properties of Fe^{3+} and Fe^{2+} by analyzing time evolution of some characteristic quantities in simulations and comparing some characteristic quantities of Fe^{3+} and Fe^{2+}. In this chapter, when comparing the characteristic quantities of the hydrogel with Fe^{3+} and Fe^{2+}, we focus on the simulations with 1250 Fe^{3+} and 1250 Fe^{2+}. We also analyze the dependence of some characteristic quantities on the Fe^{3+}/A fraction. We will see that our model captures all properties that were mentioned in Section 1.3 except that the coordination numbers of Fe^{2+} are relatively large compared to experimental observations [8-9].

6.1 COORDINATION PROPERTIES

Figure 6.2 and Figure 6.3 show the time evolution of fractions of 1250 Fe^{3+} ions and 1250 Fe^{2+} ions that are bound to different numbers of the A groups. We see that, in equilibrium, there is about 80% Fe^{3+} ions bound to two or three A groups, about 18% Fe^{3+} ions bound to one or four A groups and there are very few Fe^{3+} ions bound to zero or five A groups. Coordination numbers of most of Fe^{3+} ions are two or three. Coordination numbers of most Fe^{2+} are one and two. In the experiments [8-9], the binding interaction between Fe^{2+} and A groups is weak and the two groups are easily dissociated. The coordination numbers of Fe^{2+} in the Model II are relatively large compared to the experimental results but they still qualitatively reflect the reality, in the sense that the coordination numbers of Fe^{2+} are smaller than those of Fe^{3+}. More importantly, it is useful to examine the effects of Fe^{3+} on elastic behavior of the hydrogel for the case when Fe^{2+} can bind to A groups.

In Figure 6.4a we present the distribution of coordination numbers for 1250 Fe^{3+} and 1250 Fe^{2+} after 20 ns of the binding simulation. The coordination numbers of Fe^{3+} vary from 0 to 5 with the average of 2.5. Coordination numbers of Fe^{2+} are between 0 and 3 with the average of 1.7.

For all proportions of Fe^{3+}/A, the coordination numbers of Fe^{3+} and Fe^{2+} lie between 0 to 5 and 0 to 3, respectively. The average coordination of Fe^{3+} in equilibrium decreases from 2.8 to 2.1, as

shown in Figure 6.5. The average coordination number of Fe^{2+} varies between 1.8 and 1.6.

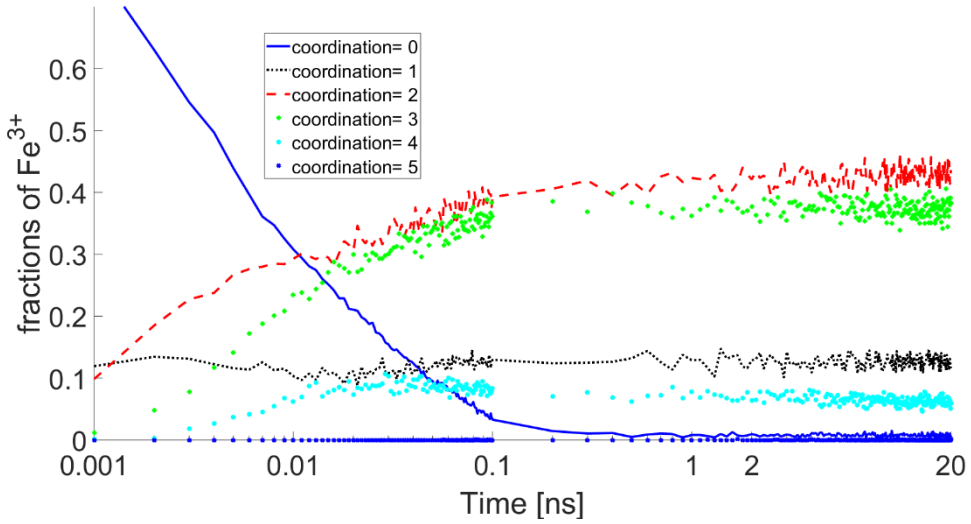

Figure 6.2. Time evolution of fractions of 1250 Fe^{3+} that are bound to different numbers of reactive groups: zero (solid blue curve), one (dotted black), two (dashed red), three (green pluses), four (cyan stars, five (blue crosses).

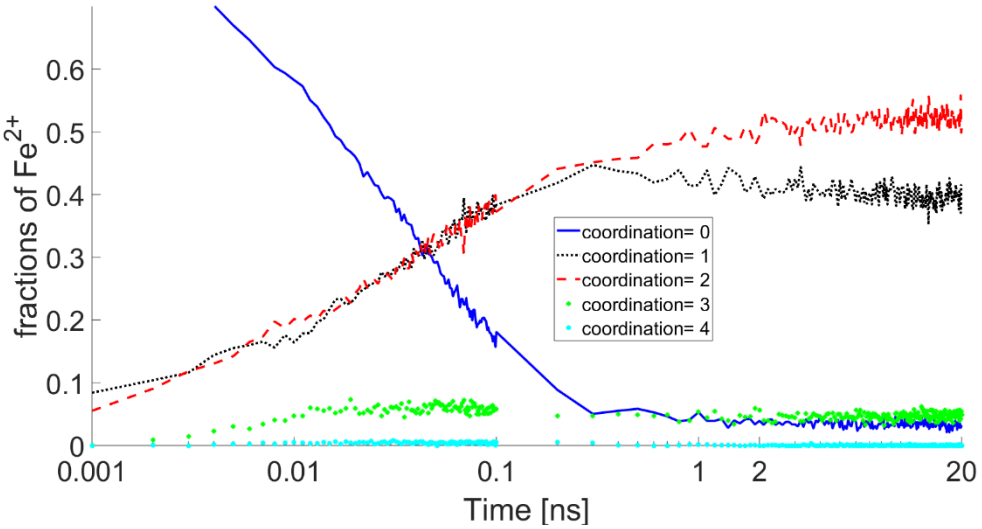

Figure 6.3. Time evolution of fractions of 1250 Fe^{2+} that are bound to different numbers of reactive groups: zero (solid blue curve), one (dotted black), two (dashed red), three (green pluses), four (cyan stars).

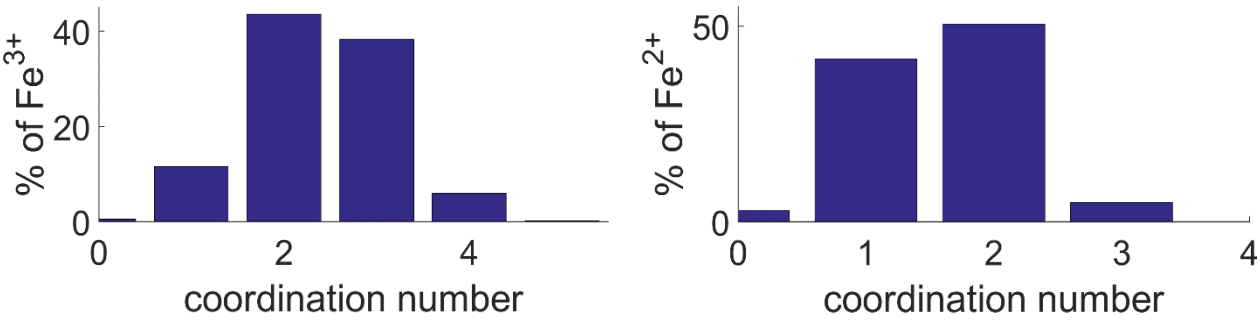

(a) (b)

Figure 6.4. Distribution of coordination number for Fe ions at the end of the binding process. (a)1250 Fe^{3+} (b)1250 Fe^{2+}

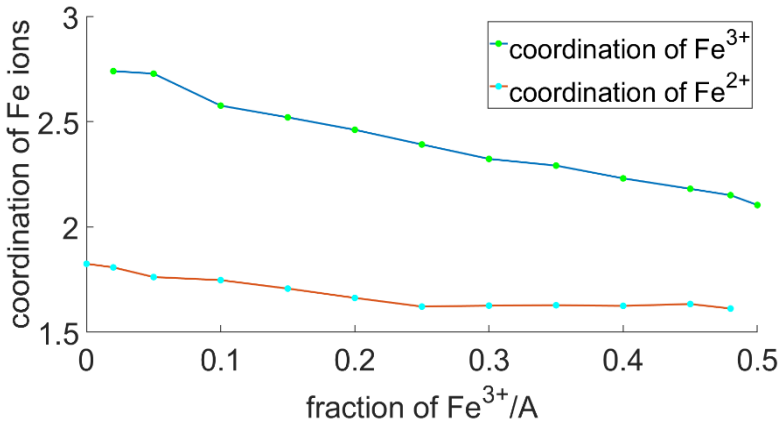

Figure 6.5. Average coordination number of Fe^{3+} (blue) and Fe^{2+} (red) with the change of the Fe^{3+}/A fraction

We observe Fe^{3+} ions "competing" to attract A groups. As the fraction of Fe^{3+}/A increases, the average of number of A groups available for one Fe^{3+} becomes smaller, and similarly to Model I, for all simulations of different Fe^{3+}/A fractions, there are very few free Fe^{3+} ions. In the Model II, although the number of complex components increases as the Fe^{3+}/A fraction increases (see

Section 6.4), the coordination numbers of Fe^{3+} still decreases. However, coordination number of Fe^{3+} is always larger than that of Fe^{2+}.

6.2 DYNAMICS OF METAL CROSSLINKS

Similarly to Model I, to monitor the strength of the crosslinks, we divide the 20 ns duration of the binding simulation into 200 time intervals, each of 100 ps duration, and calculate the total number of the crosslinks and the numbers of retained, broken and newly formed crosslinks after each 100 ps. We show the time evolution of these four quantities for the simulation with 1250 Fe^{3+} and 1250 Fe^{2+} in Figures 6.6 and 6.7. We see that all four numbers quickly approach the equilibrium values after 0.2 ns for both Fe^{3+} and Fe^{2+}. The total number of crosslinks of Fe^{3+} is larger, and the number of broken and the number of newly formed crosslinks is approximately 32% and 40% of the total number of crosslinks for Fe^{3+} and Fe^{2+}, correspondingly. So, in each 100 ps, the Fe^{2+} crosslinks are more easily dissociated.

6.3 COMPLEX COMPONENTS

In Figure 6.8a, we present the distribution of the number of Fe^{3+}/Fe^{2+} bound to a single A group for 1250 Fe^{3+} and 1250 Fe^{2+} at the end of binding process. In this Model, we see that there is about 17% A groups bound to two Fe ions. In Figure 6.8b, we see that the average number of Fe ions bound to a single A group increases from 1.06 to 1.26 as the Fe^{3+}/A fraction grows. This is in agreement with the results that there are complex components in the experiments [8-9]. We see that in the Model II, the number of complex components is larger than in the Model I.

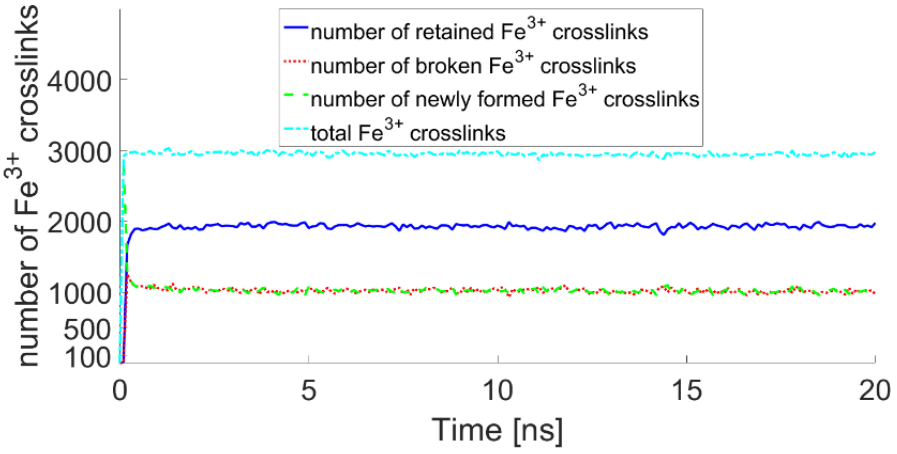

Figure 6.6. Time evolution of number of crosslinks of different types during each 100 ps subinterval for simulation of 1250 Fe^{3+}: retained (solid blue), broken (dotted red), newly formed (dashed green), and total (dash-dotted cyan) crosslinks.

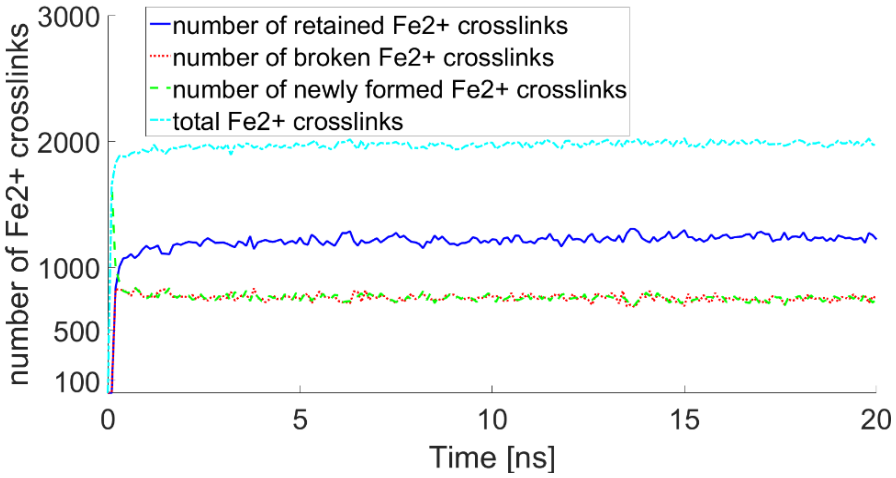

Figure 6.7. Time evolution of number of crosslinks of different types during each 100 ps subinterval for simulation of 1250 Fe^{2+}: retained (solid blue), broken (dotted red), newly formed (dashed green), and total (dash-dotted cyan) crosslinks.

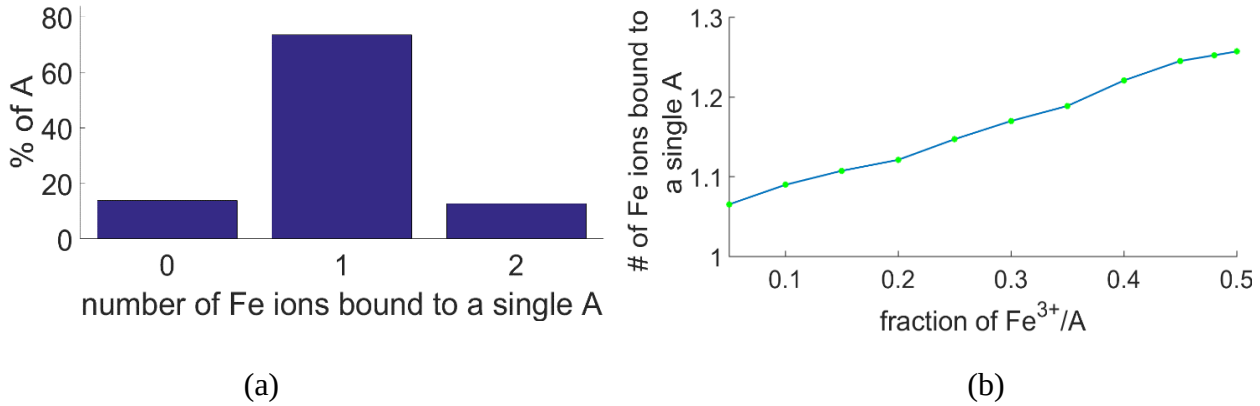

(a) (b)

Figure 6.8. Number of Fe ions bound to a single A group: (a) the distribution of number of Fe^{3+} or Fe^{2+} bound to a single A group for 1250 Fe^{3+} and 1250 Fe^{2+} at the end of binding process . (b) the average number of Fe^{3+}/Fe^{2+} bound to a single A group at the end of binding process for different Fe^{3+}/A ratio.

6.4 COMPACTION WITH FE-HYDROGEL

Similarly to Chapter 4, we use the dimension of simulation cell in order to analyze the size of the hydrogel. When there is no Fe added to the hydrogel, the dimension of the hydrogel is 13.4 nm. The dimension contracts to 12.2 nm when we add 2500 Fe^{2+}. It contracts more when the Fe^{3+}/A ratio increases, as shown in Figure 6.9. So in this model, the addition of Fe^{2+} makes the hydrogel contract. This reflects a property we mentioned in Section 1.3.

As in Model I, in order to further understand the contraction of the hydrogel, we also analyze the number of bridging Fe and the number of short loops and the number of long loops. In Figure 6.10b, we see that the total number of loops barely changes as the Fe^{3+}/A fraction grows from 0 to 0.5. This property is different from Model I. The reason is that both Fe^{3+} and Fe^{2+} create loops. However, as the Fe^{3+}/A fraction increases, the number of long loops increases (Figure 6.10b). So we see that in the Model II, Fe^{3+} ions create more long loops. We do not have detailed information about the loops in experiments but this property indicates the difference between Fe^{3+} and Fe^{2+} in

the formation of temporary loops in the hydrogel, which is related to its compaction.

Now we analyze the bridging Fe ions in the hydrogel. As shown in Figure 6.10a, the number of bridging Fe^{3+} changes from 0 to 290 as the Fe^{3+}/A fraction increases, but there are only at most 4 bridging Fe^{2+}. So in the mixture of Fe^{3+} and Fe^{2+}, both of which can form bonds, there are still very few bridging Fe^{2+}.

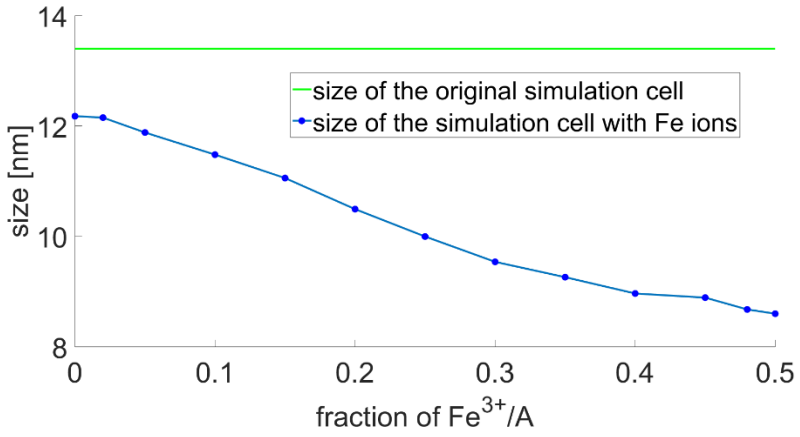

Figure 6.9. The size of the simulation cell as the Fe^{3+}/A fraction grows

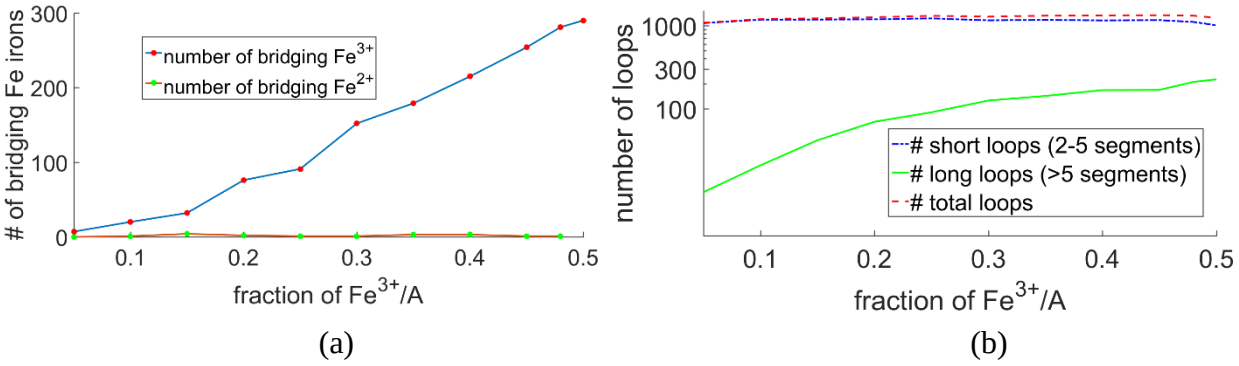

Figure 6.10. The number bridging Fe ions and the number of loops. (a) The number of bridging Fe^{3+} (blue) and bridging Fe^{2+} (red) as Fe^{3+}/A fraction is varied. (b) The number of loops created by both Fe^{3+} and Fe^{2+} as the function of Fe^{3+}/A fraction: short loops (dash dotted blue), large

6.5 ELASTIC MODULUS

Figure 6.11 shows the elastic modulus of the hydrogel under the uniaxial deformation as the Fe^{3+}/A fraction increase. The modulus in our simulations increases significantly as the Fe^{3+}/A and Fe^{3+}/Fe^{2+} fractions increase. This is in a qualitative agreement with experimental results [8-9] shown in Figure 1.2.

Similarly to Model I, in order to explain the increase in the elastic modulus as the density of Fe^{3+}/A increases, we analyze the effects of bridging Fe and bound Fe. As shown in Figure 6.12a, Fe ions are distributed roughly uniformly along each chain, similarly to Model I. In Model II, we see that the average number of units in the effective chains (segments of the original chains) at the equilibrium state in the simulations increases slowly with growing Fe^{3+}/A fractions, as shown in

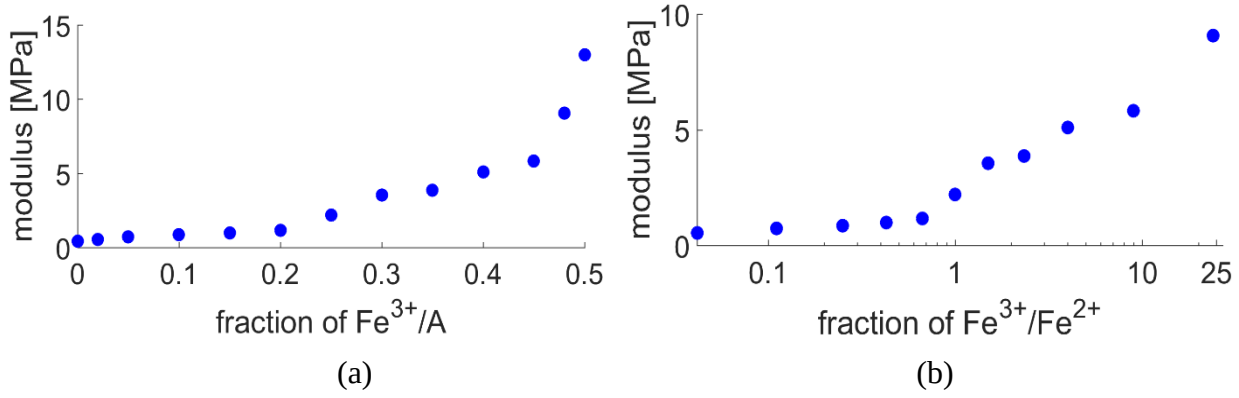

Figure 6.11. Elastic modulus of the hydrogel as (a) Fe^{3+}/A and (b) Fe^{3+}/Fe^{2+} fractions are varied.

Figure 6.12b. However, the elastic modulus increases. This is due to the bridging Fe ions. As shown in Figure 6.13a, for 1250 Fe^{3+} and 1250 Fe^{2+}, the bridging Fe ions result in 39% chains bound to one chain and 6% chains bound to two chains. The total proportion of crosslinked chains is 45%. Figure 6.13b shows that both the percentage of crosslinked chains and the number of chains bound to a single chain increase with the growth of the Fe^{3+}/A fraction. As shown in Figure 6.10a, the number of bridging Fe increases with the Fe^{3+}/A fraction. This makes the hydrogel

stiffer when the number of Fe^{3+} is increased.

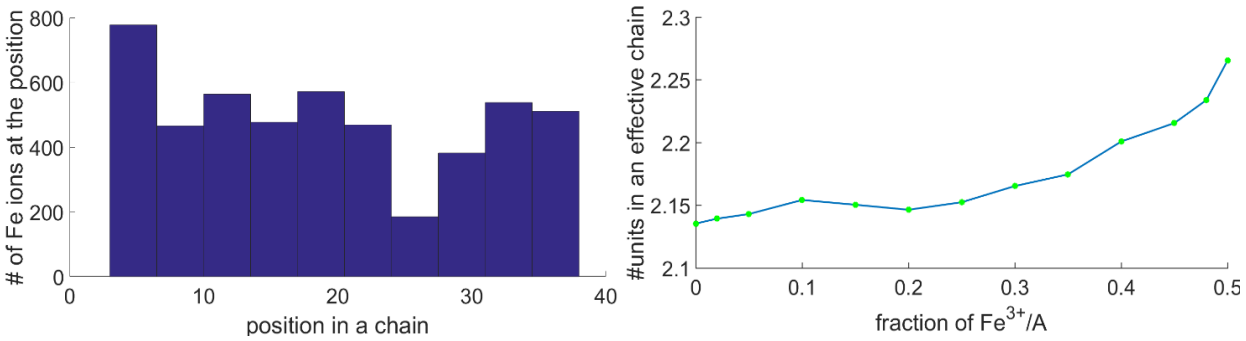

(a) (b)

Figure 6.12. The shortening of the effective chains by Fe ions. (a) Histogram of Fe position in a chain at the end of the binding process in the simulation of 1250 Fe^{3+} and 1250 Fe^{2+} (b) Average number of units in an effective chain.

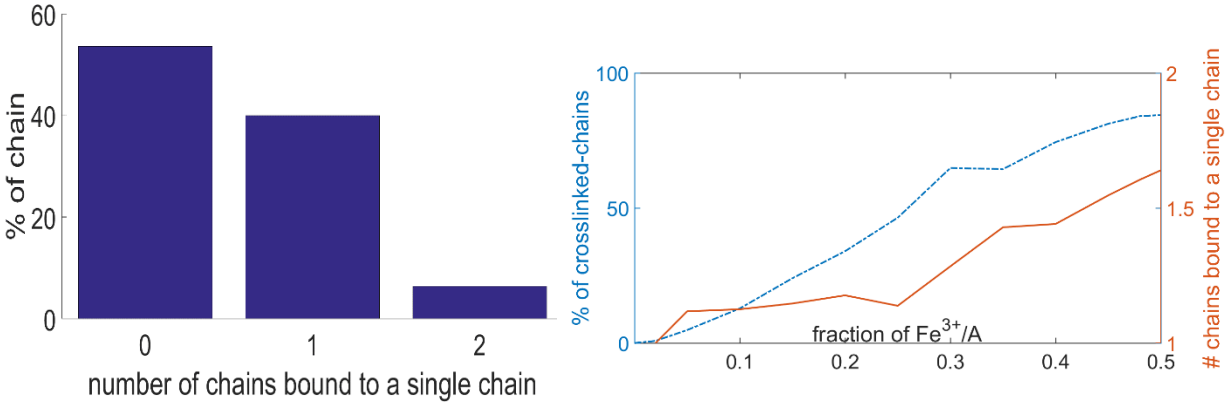

(a) (b)

Figure 6.13. The number of chains bound to a single chain. (a) Histogram of percentage of chains in the hydrogel bound to number of different chains at the end of the binding process in the simulation of 1250 Fe^{3+} and 1250 Fe^{2+} (b) Percentage of crosslinked-chain (dash dotted blue, left y-axis), and average number of chains bound to a single chain (solid orange, right y-axis)

7.0 SUMMARY, CONCLUSIONS AND DISCUSSION

7.1 SUMMARY

Experimental observations [8] show that upon the addition of metals Fe^{3+} or Fe^{2+} to the hydrogel, the sodium acrylate groups (reactive groups A) of the covalent network can form strong additional crosslinks with Fe^{3+} and weak crosslinks with Fe^{2+}. Experiments suggest the changes in modulus and size of the hydrogels could be explained by a change in crosslink density due to the higher affinity of Fe^{3+} for carboxylate (chemical compound contained in group A) compared with Fe^{2+}. To better understand the internal structure of the hydrogel and explain the effects of metal crosslinkers on the behavior of the hydrogels, we developed and studied two computational models that include the same permanent polymeric network and different type of crosslinkers.

In Model I, Fe^{2+} are considered non-binding. This model qualitatively reflects some of the observed properties, including the significant growth of the elastic modulus and the compaction when the number of Fe^{3+} increases. The coordination numbers of Fe^{3+} are also in a realistic range. However, the Model I does not reflect the compaction of Fe^{2+}-hydrogel.

Our Model II accounts for a hydrogel in the presence of two different types of crosslinkers. Fe^{3+} ions bind strongly to the reactive groups, while the bonds made by Fe^{2+} are weaker. The Model II reflects all experimentally observed chemical properties except that the coordination number of Fe^{2+} is not sufficiently small in comparison with experimental results [8-9].

To study the effects of Fe^{3+} and Fe^{2+}, we ran the simulations where the overall number of Fe ions was fixed but the Fe^{3+}/A fraction was varied from 0 to 0.5 in different runs, and consequently Fe^{2+}/A fraction was varied as well. Then we calculated and analyzed the characteristic quantities such as the elastic modulus, the size of the simulation cell, the coordination numbers, the number

of bridging crosslinkers, the number of loops, etc.

In the two models, the dependence of elastic modulus on the Fe^{3+}/Fe^{2+} and Fe^{3+}/A fractions obtained in our simulations is qualitatively similar to the experimental results of [8-9] shown in Figure 1.2. To understand why the elastic modulus increases with the proportion of Fe^{3+}/A, we investigated the effects of bound Fe ions and bridging crosslinkers. We demonstrated that the effective length of the original chains becomes shorter when we add Fe^{3+} in the Model I and Fe^{3+} and Fe^{2+} to the hydrogel. The number of bridging Fe, the percentage of crosslinked-chains and the number of chains bound to a single chain increase with the Fe^{3+}/A fraction. Both the shorter effective chains and the crosslinks of chains contribute to make the hydrogel stiffer.

As the Fe^{3+}/A fraction increases, the number of loops increases significantly. The number of bridging Fe^{3+} is small comparing to the number of A groups, but together with the loops, they make the average distance between the groups significantly shorter when the Fe^{3+}/A fraction increases. This explains the compaction of the hydrogel when more Fe^{3+} are added in the simulations.

7.2 CONCLUSIONS

The change in the elastic modulus is due to two effects of crosslinkers: the effective shortening of chains due to loops and local contraction and the chain crosslinking. These two effects are due to the bound crosslinkers and bridging crosslinkers, respectively. By comparing the two effects for one type of crosslinker (Fe^{3+} in Model I), and a mixture of two types of crosslinkers (Fe^{3+} and Fe^{2+} in Model II), we found that the increase of number of bridging crosslinkers is the main factor responsible for the significant increase modulus of the hydrogel.

Our models suggest that the difference between the number of bridging Fe^{3+} and bridging Fe^{2+} in the hydrogel significantly affects the elastic modulus of the hydrogel when the Fe^{3+}/A fraction changes. In the simulations of the Model II, there are always very few bridging Fe^{2+} in the hydrogel

even if the Fe^{2+}/A fraction is 0.5. The addition of Fe^{2+} to hydrogel makes the length of effective chains shorter instead of increasing the number of bridging Fe^{2+}. On the other hand, the number of bridging Fe^{3+} is a monotonely increasing function of Fe^{3+}/A.

7.3 DISCUSSION AND FUTURE WORK

7.3.1 Effect of water and suggestion to improve the Model II

In Model II, the coordination numbers of Fe^{2+} are not sufficiently small compared to the experiments [8-9]. Unfortunately, among the types of crosslinkers we considered in Chapter 5, the parameters we found for Fe^{2+} in Model II was our best choice.

To eliminate this deficiency of the Model II, we need a model of hydrogel in which the strength of Fe^{2+}-A crosslinks are reduced but the Fe^{2+}-hydrogel is still contracted. This suggests reevaluating how the solvent of the hydrogel is represented. In our model, there are some factors that reflect the presence of water (see Section 2.1.7). However, the effect of water on temporary crosslinks may not be modelled sufficiently well. Water can reduce the attractive forces between Fe^{2+} ions and A groups while the binding forces may be still strong enough to make the hydrogel contract.

In order to mimic the effect of water or other solvents, as mentioned in Section 1.2.2, currently we have several options. We can use the popular implicit solvation models such as Born or Still models [41, 86]. Or we can add friction forces to particles in the hydrogel and control their strengths. Adding friction forces is more useful when modeling hydrogels with different weights of monomers, which is the case our models (see Section 2.1.5). We can apply friction forces for particles by using Brownian Dynamics. GROMACS offers both popular implicit solvent models and Brownian Dynamics in the simulation package. In the future simulations, we will use these solvent models and compare the results with the findings in this thesis.

7.3.2 Modulus of the original hydrogel

The moduli of the hydrogel without Fe ions in chemical experiments [8-9] and our simulations are 0.038 MPa and 0.16 MPa, respectively. In [8-9], the modulus is 2.7 MPa with the fraction Fe^{3+}/A of 0.45 while the corresponding values in Model I and model II are 23.72 MPa and 5.81 MPa, respectively. Our model qualitatively reflects the significant increase of the modulus when we add Fe^{3+} but in order to get the modulus of the hydrogel with Fe^{3+} closer to the experimentally measured value, we need to simulate an original hydrogel with smaller modulus. We could simulate a covalent network with fewer chains (about 200 chains instead of 250 chains) and smaller crosslink functionalities (as in Chapter 1, the crosslink functionality of a PEG-DA group is defined by the number of chains bound to that PEG-DA). In such a hydrogel, the permanent crosslink density should decrease, making the original hydrogel softer. To get a hydrogel network with a smaller maximum functionality, we could apply a simulation process in [108]. These simulations for softer hydrogel will be performed in the future work.

7.3.3 Simulations for other experiments

There are other experiments related to hydrogel with metal crosslinks [74, 77]. We can build models to reflect and explain these experiments. We first need the information of covalent networks and crosslinkers to model the topology and geometry of polymer network by setting suitable interaction potentials as in Chapter 2.

7.3.4 Running the simulations for different networks

In our thesis, due to many running processes with long time scales, we mainly run the simulations in the same covalent network. In the future, we can perform the simulations for other permanent networks.

APPENDIX

SUPPLEMENTARY MATERIAL

In this appendix, we provide further details about our simulations in GROMACS. Specifically, we include the following:

-The matlab code to generate the tables of WCA and Morse potentials

-The mdp files for the simulation steps we illustrate in Figure 2.2

-The topology files of the first two steps in Figure 2.2

We only include the topology files of the first two steps when the topology of system can be represented as the regular chains and groups. When the network formed, it is treated as one large molecule in an irregular order of A and S. We need to provide information for all bonded-interaction potentials (including harmonic bonding and bond angle potentials) separately. Therefore, the topology files of these simulation steps are too long (about one thousand pages for one file) to show here. Readers interested in these files should contact the author at htn3@pitt.edu. In the mdp and topology files, we denote A as E, S and PEG-DA as M, Fe^{3+} as X, Fe^{2+} as Z.

A.1 THE MATLAB CODE

A.1.1 The Matlab code to generate the table of WCA potential

```
%This program generates the table of WCA potential for GROMACS

cutoff=0.30;%the quilibrium distance between the two groups P and Q
            %other parameters are set in the topology file

fid = fopen('table_P_Q.xvg','w');

fprintf(fid,'%s\n%s\n%s%s\n','#','#WCA ','#cut-off at ',num2str(cutoff));

for i=0:3
    r=0.0005*i;
    fprintf(fid,
'%11.10e%s%11.10e%s%11.10e%s%11.10e%s%11.10e%s%11.10e%s%11.10e%\n',r,'
',0,' ',0,'   ',0,' ',0,'   ', 0,' ',0);
    fprintf(fid,'\n');
end

num=floor(cutoff/0.0005);

for i=4:(num-1)
    r=0.0005*i;
    f=1/r;
    df=1/r^2;
    g=-1/r^6;
    dg=-6/r^7;
    h=1/r^12;
    dh=12/r^13;
    fprintf(fid,
'%11.10e%s%11.10e%s%11.10e%s%12.10e%s%11.10e%s%11.10e%s%11.10e%\n',r,'
',0,' ',0,'   ',g,' ',dg,'   ', h,' ',dh);
    fprintf(fid,'\n');
end

for i=num:6000
    r=0.0005*i;
    fprintf(fid,
'%11.10e%s%11.10e%s%11.10e%s%11.10e%s%11.10e%s%11.10e%s%11.10e%\n',r,'
',0,' ',0,'   ',0,' ',0,'   ', 0,' ',0);
    fprintf(fid,'\n');
end

fclose(fid);
```

A.1.2 The Matlab code to generate the table of Morse potential

```
%This program generates the table of Morse potential for GROMACS

b=0.12;     %equilibrium distance
beta=120;   %width control coefficient
            %The parameter D is set in the topology file

fid = fopen('table.xvg','w');

fprintf(fid,'%s\n%s%s\n%s%s\n','#Morse potential','#equilibrium bond
distance= ',num2str(b),'#width control coefficient= ',num2str(beta));

for i=0:5000
    r=0.0005*i;
    h=1+exp(-2*beta*(r-b))-2*exp(-beta*(r-b));
    dh= 2*beta*exp(-2*beta*(r-b))-2*beta*exp(-beta*(r-b));
    fprintf(fid,
'%11.10e%s%11.10e%s%11.10e%s%11.9e%s%11.10e%s%11.10e%s%11.10e%\n',r,'    ',0,'
',0,'    ',-1,' ',0,'    ', h,' ',dh);
    fprintf(fid,'\n');
end

for i=5001:6000
    r=0.0005*i;
    fprintf(fid,
'%11.10e%s%11.10e%s%11.10e%s%11.10e%s%11.10e%s%11.10e%s%11.10e%s%11.10e%\n',r,'
',0,' ',0,'    ',-1,' ',0,'    ', 1,' ',0);
    fprintf(fid,'\n');
end

fclose(fid);
```

A.2 THE MDP FILES

A.2.1 Network formation: Mixing step (NVT)

```
title       = Network formation, mixing

integrator              = md
dt                      = 0.002
nsteps                  = 5000000


nstxout                 = 25000
nstvout                 = 25000
nstlog                  = 25000
nstenergy               = 2500
nstxtcout               = 2500

energygrps              = E M X
energygrp_table         = E E E M E X M M M X X X

nstlist                 = 10
ns_type                 = grid
rlist                   = 1.0

vdwtype                 = User
coulombtype             = Cut-off

rcoulomb                = 1.0
rvdw                    = 1.0


tcoupl                  = berendsen
tc-grps                 = system
tau_t                   = 0.1
ref_t                   = 300
```

A.2.2 Network formation: Binding step (NPT)

```
title                    =Network formation, binding

integrator               = md

dt                       = 0.001
nsteps                   = 400000000

nstxout                  = 50000
nstvout                  = 50000
nstlog                   = 50000
nstenergy                = 5000
nstxtcout                = 5000

energygrps               = E M X
energygrp_table          = E E E M E X M M M X X X

nstlist                  = 10
ns_type                  = grid
rlist                    = 1.0

vdwtype                  = User
coulombtype              = Cut-off

rcoulomb                 = 1.0
rvdw                     = 1.0

tcoupl                   = berendsen
tc-grps                  = system
tau_t                    = 0.1
ref_t                    = 300

Pcoupl                   = berendsen
Pcoupltype               = isotropic
tau_p                    = 1.0 ;5.0
compressibility          = 4.5e-5
ref_p                    = 1.0
```

A.2.3 Network formation: Reconstructing step (NPT)

```
title                    = Network formation, reconstructing

integrator               = md

dt                       = 0.0002
nsteps                   = 1000000000

nstxout                  = 100000
nstvout                  = 100000
nstlog                   = 200000
nstenergy                = 10000
nstxtcout                = 10000

energygrps               = E M
energygrp_table          = E E E M M M

nstlist                  = 10
ns_type                  = grid
rlist                    = 1.0
vdwtype                  = User
coulombtype              = Cut-off

rcoulomb                 = 1.0
rvdw                     = 1.0

tcoupl                   = berendsen
tc-grps                  = system
tau_t                    = 0.1
ref_t                    = 300

Pcoupl                   = berendsen
Pcoupltype               = isotropic
tau_p                    = 1.0
compressibility          = 4.5e-5
ref_p                    = 1.0
```

A.2.4 Network formation: Relaxation step (NVT)

```
title                    = Network formation, relaxation

integrator               = md

dt                       = 0.001
nsteps                   = 10000000

nstxout                  = 100000
nstvout                  = 100000
nstlog                   = 200000
nstenergy                = 100
nstxtcout                = 100

energygrps               = E M
energygrp_table          = E E E M M M

nstlist                  = 10
ns_type                  = grid
rlist                    = 1.0

vdwtype                  = User
coulombtype              = Cut-off


tcoupl                   = berendsen
tc-grps                  = system
tau_t                    = 0.1
ref_t                    = 300
```

A.2.5 Mixing Fe ions to the hydogel (NVT)

```
title                    = Mixing Fe

integrator               = md
dt                       = 0.002
nsteps                   = 5000000

nstxout                  = 50000
nstvout                  = 50000
nstlog                   = 200000
nstenergy                = 5000
nstxtcout                = 5000

energygrps               = E M X Z
energygrp_table          = E E E X M X X X X Z Z Z M Z E Z

nstlist                  = 10
ns_type                  = grid
rlist                    = 1.4

vdwtype                  = User
coulombtype              = Cut-off

tcoupl                   = berendsen
tc-grps                  = system
tau_t                    = 0.1
ref_t                    = 300
```

A.2.6 Temporary crosslink formation (NPT)

```
title                    = Binding Fe-A crosslinks

integrator               = md
dt                       = 0.001
nsteps                   = 20000000
nstxout                  = 1000
nstvout                  = 1000
nstlog                   = 200000
nstenergy                = 10000
nstxtcout                = 10000

energygrps               = E M X Z
energygrp_table          = E E E X M X X X X Z Z Z M Z E Z

nstlist                  = 10
ns_type                  = grid
rlist                    = 1.2
rvdw_switch              = 0.9

vdwtype                  = User
coulombtype              = cut-off
rcoulomb                 = 1.2
rvdw                     = 1.0

tcoupl                   = berendsen
tc-grps                  = system
tau_t                    = 0.1
ref_t                    = 300
energygrps               =

Pcoupl                   = berendsen
Pcoupltype               = isotropic
tau_p                    = 1.0 ;5.0
compressibility          = 4.5e-5
ref_p                    = 1.0
```

A.2.7 Hydrogel relaxation (NVT)

```
title                    = Hydrogel relaxation

integrator               = md
dt                       = 0.002
nsteps                   = 2500000

nstxout                  = 25000
nstvout                  = 25000
nstlog                   = 200000
nstenergy                = 1
nstxtcout                = 0

xtc_grps                 =
energygrps               = E M X Z
energygrp_table          = E E E X M X X X X Z Z Z M Z E Z

nstlist                  = 10
ns_type                  = grid
rlist                    = 1.2

vdwtype                  = User
coulombtype              = Cut-off
rcoulomb                 = 1.2

tcoupl                   = berendsen
tc-grps                  = system
tau_t                    = 0.1
ref_t                    = 300


gen_vel                   = no
gen_temp                  = 300
gen_seed                  = 173529
```

A.2.8 Hydrogel deformation (Non-equilibrium MD)

```
;The parameter deform must be calculated for each deformation step

title                    = hydrogel deforming

integrator               = md
dt                       = 0.002
nsteps                   = 250000

nstxout                  = 2500
nstvout                  = 2500
nstlog                   = 2500
nstenergy                = 2500
nstxtcout                = 2500

energygrps               = E M X Z
energygrp_table          = E E E X M X X X X Z Z Z M Z E Z

nstlist                  = 10
ns_type                  = grid
rlist                    = 1.2

vdwtype                  = User
coulombtype              = Cut-off

rcoulomb                 = 1.2
rvdw                     = 1.0

tcoupl                   = berendsen
tc-grps                  = system
tau_t                    = 0.1
ref_t                    = 300

deform                   =-0.0004846704  -0.0004846704  0.0010  0  0  0
```

A.3 TOPOLOGY FILES

A.3.1 Network formation: Mixing step (NVT)

```
; This is the topology file for step 1

; Include forcefield parameters
[ defaults ]
; nbfunc    comb-rule   gen-pairs   fudgeLJ fudgeQQ
  1         1           no          0       0

[ atomtypes ]
;name at.num  mass charge  ptype    c6      c12                 rm    epsilon
X   6   183.00    0.0   A   1.4373508E-03    1.321116272E-06   ;0.35    0.391
E   6   183.00    0.0   A   5.7000942E-04    2.077684339E-07   ;0.30    0.391
M   6   183.00    0.0   A   6.4927635E-03    2.695719318E-05   ;0.45    0.391

[ nonbond_params ]
; i   j  func       c6                   c12                rm       epsilon
X   E       1       2.3347586E-06       3.485775893E-12     ;0.12      0.391
E   E       1       5.7000942E-04       2.077684339E-07     ;0.30      0.391
M   M       1       6.4927636E-03       2.695719342E-05     ;0.45      0.391
X   X       1       1.4373508E-03       1.321116272E-06     ;0.35      0.391
E   M       1       6.4927636E-03       2.695719342E-05     ;0.45      0.391
M   X       1       8.8652419E-05       5.025701374E-09     ;0.22      0.391

[ bondtypes ]
; i     j      func      b0    Kb_bolton
  E     M      1         0.3    376141.6
  M     M      1         0.4    376141.6
  E     E      1         0.2    376141.6

[ moleculetype ]
; Name            nrexcl
CH                3

[ atoms ]
;   nr       type  resnr residue  atom   cgnr      charge       mass
     1          E      1     CH     E       1          0     72.0000
     2          M      1     CH     M       2          0     183.00
     3          M      1     CH     M       3          0     183.00
     4          M      1     CH     M       4          0     183.00
     5          M      1     CH     M       5          0     183.00
     7          M      1     CH     M       7          0     183.00
     8          M      1     CH     M       8          0     183.00
     9          M      1     CH     M       9          0     183.00
    10          M      1     CH     M      10          0     183.00
    11          M      1     CH     M      11          0     183.00
    12          M      1     CH     M      12          0     183.00
    13          M      1     CH     M      13          0     183.00
    14          M      1     CH     M      14          0     183.00
    15          M      1     CH     M      15          0     183.00
    16          M      1     CH     M      16          0     183.00
    17          M      1     CH     M      17          0     183.00
    18          M      1     CH     M      18          0     183.00
```

```
    19          M      1     CH     M      19          0     183.00
    20          M      1     CH     M      20          0     183.00
    21          M      1     CH     M      21          0     183.00
    22          M      1     CH     M      22          0     183.00
    23          M      1     CH     M      23          0     183.00
    24          M      1     CH     M      24          0     183.00
    25          M      1     CH     M      25          0     183.00
    26          M      1     CH     M      26          0     183.00
    27          M      1     CH     M      27          0     183.00
    28          M      1     CH     M      28          0     183.00
    29          M      1     CH     M      29          0     183.00
    30          M      1     CH     M      30          0     183.00
    31          M      1     CH     M      31          0     183.00
    32          M      1     CH     M      32          0     183.00
    33          M      1     CH     M      33          0     183.00
    34          M      1     CH     M      34          0     183.00
    35          M      1     CH     M      35          0     183.00
    36          M      1     CH     M      36          0     183.00
    37          M      1     CH     M      37          0     183.00
    38          M      1     CH     M      38          0     183.00
    39          M      1     CH     M      39          0     183.00
    40          E      1     CH     E      40          0     72.0000

[ bonds ]
;  ai    aj funct
    1     2     1
    2     3     1
    3     4     1
    4     5     1
    5     6     1
    6     7     1
    7     8     1
    8     9     1
    9    10     1
   10    11     1
   11    12     1
   12    13     1
   13    14     1
   14    15     1
   15    16     1
   16    17     1
   17    18     1
   18    19     1
   19    20     1
   20    21     1
   21    22     1
   22    23     1
   23    24     1
   24    25     1
   25    26     1
   26    27     1
   27    28     1
   28    29     1
   29    30     1
   30    31     1
   31    32     1
   32    33     1
```

```
   33    34     1
   34    35     1
   35    36     1
   36    37     1
   37    38     1
   38    39     1
   39    40     1

[ angles ]
;  ai    aj    ak funct
    1     2     3     2
    2     3     4     2
    3     4     5     2
    4     5     6     2
    5     6     7     2
    6     7     8     2
    7     8     9     2
    8     9    10     2
    9    10    11     2
   10    11    12     2
   11    12    13     2
   12    13    14     2
   13    14    15     2
   14    15    16     2
   15    16    17     2
   16    17    18     2
   17    18    19     2
   18    19    20     2
   19    20    21     2
   20    21    22     2
   21    22    23     2
   22    23    24     2
   23    24    25     2
   24    25    26     2
   25    26    27     2
   26    27    28     2
   27    28    29     2
   28    29    30     2
   29    30    31     2
   30    31    32     2
   31    32    33     2
   32    33    34     2
   33    34    35     2
   34    35    36     2
   35    36    37     2
   36    37    38     2
   37    38    39     2
   38    39    40     2

[ moleculetype ]
; Name            nrexcl
XXX               1

[ atoms ]
;   nr       type  resnr residue  atom   cgnr     charge       mass
     1          X      1     XXX   X      1       0.00     55.845
```

```
[ system ]
; Name
Hello

[ molecules ]
; Compound        #mols
CH                 250
XXX                250
```

A.3.2 Network formation: Binding step (NPT)

```
; This is the topology file for step 1

; Include forcefield parameters
[ defaults ]
; nbfunc    comb-rule   gen-pairs   fudgeLJ fudgeQQ
  1         1           no          0       0

[ atomtypes ]
;name at.num  mass charge  ptype    c6      c12             rm    epsilon
X   6   183.00    0.0   A   1.4373508E-03    1.321116272E-06   ;0.35    0.391
E   6   183.00    0.0   A   5.7000942E-04    2.077684339E-07   ;0.30    0.391
M   6   183.00    0.0   A   6.4927635E-03    2.695719318E-05   ;0.45    0.391

[ nonbond_params ]
; i   j  func       c6                  c12                rm       epsilon
X   E       1       150                 150                ;0.12      0.391
E   E       1       5.7000942E-04       2.077684339E-07    ;0.30      0.391
M   M       1       6.4927636E-03       2.695719342E-05    ;0.45      0.391
X   X       1       1.4373508E-03       1.321116272E-06    ;0.35      0.391
E   M       1       6.4927636E-03       2.695719342E-05    ;0.45      0.391
M   X       1       8.8652419E-05       5.025701374E-09    ;0.22      0.391

[ bondtypes ]
; i     j      func      b0    Kb_bolton
  E     M      1         0.3    376141.6
  M     M      1         0.4    376141.6
  E     E      1         0.2    376141.6

[ moleculetype ]
; Name            nrexcl
CH                3

[ atoms ]
;   nr       type  resnr residue  atom   cgnr      charge       mass   typeB
     1          E      1     CH     E       1           0     72.0000
     2          M      1     CH     M       2           0     183.00
     3          M      1     CH     M       3           0     183.00
     4          M      1     CH     M       4           0     183.00
     5          M      1     CH     M       5           0     183.00
     7          M      1     CH     M       7           0     183.00
     8          M      1     CH     M       8           0     183.00
     9          M      1     CH     M       9           0     183.00
    10          M      1     CH     M      10           0     183.00
    11          M      1     CH     M      11           0     183.00
    12          M      1     CH     M      12           0     183.00
    13          M      1     CH     M      13           0     183.00
    14          M      1     CH     M      14           0     183.00
    15          M      1     CH     M      15           0     183.00
    16          M      1     CH     M      16           0     183.00
    17          M      1     CH     M      17           0     183.00
    18          M      1     CH     M      18           0     183.00
    19          M      1     CH     M      19           0     183.00
    20          M      1     CH     M      20           0     183.00
```

```
    21          M      1     CH     M      21          0     183.00
    22          M      1     CH     M      22          0     183.00
    23          M      1     CH     M      23          0     183.00
    24          M      1     CH     M      24          0     183.00
    25          M      1     CH     M      25          0     183.00
    26          M      1     CH     M      26          0     183.00
    27          M      1     CH     M      27          0     183.00
    28          M      1     CH     M      28          0     183.00
    29          M      1     CH     M      29          0     183.00
    30          M      1     CH     M      30          0     183.00
    31          M      1     CH     M      31          0     183.00
    32          M      1     CH     M      32          0     183.00
    33          M      1     CH     M      33          0     183.00
    34          M      1     CH     M      34          0     183.00
    35          M      1     CH     M      35          0     183.00
    36          M      1     CH     M      36          0     183.00
    37          M      1     CH     M      37          0     183.00
    38          M      1     CH     M      38          0     183.00
    39          M      1     CH     M      39          0     183.00
    40          E      1     CH     E      40          0     72.0000

[ bonds ]
;  ai    aj funct
    1     2     1
    2     3     1
    3     4     1
    4     5     1
    5     6     1
    6     7     1
    7     8     1
    8     9     1
    9    10     1
   10    11     1
   11    12     1
   12    13     1
   13    14     1
   14    15     1
   15    16     1
   16    17     1
   17    18     1
   18    19     1
   19    20     1
   20    21     1
   21    22     1
   22    23     1
   23    24     1
   24    25     1
   25    26     1
   26    27     1
   27    28     1
   28    29     1
   29    30     1
   30    31     1
   31    32     1
   32    33     1
   33    34     1
   34    35     1
```

```
   35    36     1
   36    37     1
   37    38     1
   38    39     1
   39    40     1

[ angles ]
;  ai    aj    ak funct
    1     2     3     2
    2     3     4     2
    3     4     5     2
    4     5     6     2
    5     6     7     2
    6     7     8     2
    7     8     9     2
    8     9    10     2
    9    10    11     2
   10    11    12     2
   11    12    13     2
   12    13    14     2
   13    14    15     2
   14    15    16     2
   15    16    17     2
   16    17    18     2
   17    18    19     2
   18    19    20     2
   19    20    21     2
   20    21    22     2
   21    22    23     2
   22    23    24     2
   23    24    25     2
   24    25    26     2
   25    26    27     2
   26    27    28     2
   27    28    29     2
   28    29    30     2
   29    30    31     2
   30    31    32     2
   31    32    33     2
   32    33    34     2
   33    34    35     2
   34    35    36     2
   35    36    37     2
   36    37    38     2
   37    38    39     2
   38    39    40     2

[ moleculetype ]
; Name            nrexcl
XXX               1

[ atoms ]
;   nr       type  resnr residue  atom   cgnr     charge       mass  typeB
     1          X      1     XXX   X      1       0.00     55.845
```

```
[ system ]
; Name
Hello

[ molecules ]
; Compound        #mols
CH                 250
XXX                250
```

BIBLIOGRAPHY

[1] Z. Alexandrowicz and Y. Accad. Monte Carlo of chains with excluded volume: distribution of intersegmental distances. *J. Chem. Phys.* **1971**, 54, 5338–5345.

[2] M. P. Allen and D. J. Tildesley. *Computer Simulations of Liquids*. Oxford University Press, **2002.**

[3] D. Althans, K. Langenbach, S. Enders (**2012**) Influence of different alcohols on the swelling behaviour of hydrogels. *Mol Phys.* 110(11–12, SI):1391–1402.

[4] T. Amiya, T. Tanaka (**1987**) Phase-transitions in cross-linked gels of natural polymers. *Macromolecules* 20(5):1162–1164.

[5] C.A. Angell (**1993**) Water-II is a strong liquid. *J Phys Chem.* 97(24):6339–6341.

[6] Singh Anisha, Sharma Pramod Kumar, Garg Vipin Kumar,Garg Garima. Hydrogels: a review. *International Journal of Pharmaceutical Sciences Review and Research.* **2010**, 4(2):Article 016. ISSN: 0976-044X.

[7] Amin Aramoon, Timothy D. Breitzman, Christopher Woodward, and Jaafar A. El-Awady. Coarse-Grained Molecular Dynamics Study of the Curing and Properties of Highly Cross-Linked Epoxy Polymers. *J Phys Chem B.* **2016** Sep 8;120(35):9495-505.

[8] J.T. Auletta, G.J. LeDonne, K.C. Gronborg, C.D. Ladd, H. Liu, W.W. Clark, and T.Y. Meyer. Stimuli-responsive iron-cross-linked hydrogels that undergo redox-driven switching between hard and soft states. *Macromolecules*. 48(6):1736-1747, **2015**.

[9] J. T. Auletta and T.Y. Meyer. *Personal communication*. **2015.**

[10] Riccardo Baron, Alex H. de Vries, Philippe H. Hünenberger, and Wilfred F. van Gunsteren (**2007**). Comparison of Thermodynamic Properties of Coarse-Grained and Atomic-Level Simulation Models. *Chem Phys Chem.* 8 (3): 452–461.

[11] H. J. C. Berendsen, J. P. M. Postma, W. F. van Gunsteren, A. DiNola, and J. R. Haak. Molecular dynamics with coupling to an external bath. *The Journal of Chemical Physics.* 81, 3684 (**1984**).

[12] J. S. Bermejo and C. M. Ugarte. Chemical crosslinking of pva and prediction of material properties by means of fully atomistic md simulations. *Macromolecular Theory and Simulations*. 18:259-267, **2009**.

[13] C. Bishop. *Pattern Recognition and Machine Learning*. Springer-Verlag. **2006.**

[14] J.O'M. Bockris and et al. *Modern Electrochemistry*, volume 1, 2nd edition. Kluwer Academic Publishers. **2002**.

[15] J.O'M. Bockris and A.K.N Reddy. *Modern Electrochemistry*, volume 2A, 2nd edition. Kluwer Academic Publishers,. **2002**.

[16] Enrica Caló, Vitaliy V. Khutoryanskiy. Biomedical applications of hydrogels: A review of patents and commercial products. *European Polymer Journal*. 65 (**2015**) 252–267.

[17] H. L. Ceperley, H. L. Frisch, M. Bishop, M.H. Kalos. Investigation of static properties of model bulk polymer fluids. *J. Chem. Phys.* **1980**, 72, 3228–3235.

[18] J. Chakrabarty (**2006**). *Theory of plasticity*, 3rd edition. Butterworth-Heinemann.

[19] Z. Chen, C. Cohen and F.A. Escobedo. Monte Carlo simulation of the effect of entanglements on the swelling and deformation of end-linked polymeric networks. *Macromolecules.* **35**, 3296-3305, **2002**.

[20] E. Chiessi, F. Cavalieri, G. Paradossi (**2007**) Water and polymer dynamics in chemically cross-linked hydrogels of poly(vinyl alcohol): a molecular dynamics simulation study. *J Phys Chem B.* 111(11):2820–2827. PMID: 17388423.

[21] C.J. Cramer, D.G. Truhlar, (**1999**). Implicit Solvation Models: Equilibria, Structure, Spectra, and Dynamics. *Chemical Reviews*. 99 (8): 2161–2200.

[22] C.J. Cramer (**2013**). *Essentials of Computational Chemistry: Theories and Models.* John Wiley & Sons.

[23] E. De Vos and A. Bellemans. Concentration dependence of the mean dimension of a polymer chain. *Macromolecules.* **1974**, 7, 812–814.

[24] J.M. Deutsch, I. Oppenheim. The concept of Brownian motion in modern statistical mechanics. *Chem. Soc.* **1987**, 83, 1–20.

[25] E. A. Di Marzio, and J. H. Gibbs. Chain Stiffness and the Lattice Theory of Polymer Phases. *J. Chem. Phys.* 28 (**1958**), 807.

[26] D.C. Doherty, B. N. Holmes, P. Leung, and R. B Ross. Polymerization molecular dynamics simulations. I. cross-linked atomistic models for poly(methacrylate) networks. *Computational and Theoretical Polymer Science*. 8:169-178, **1998**.

[27] D.L. Ermak, H. Buckholtz. Numerical integration of the Langevin equation: Monte Carlo simulation. *J. Comput. Phys.* **1980**, 35, 169–182.

[28] D.L. Ermak and Y. Yeh. Equilibrium electrostatic effects on behavior of polyions in solution: polyion–mobile ion interaction. *Chem. Phys. Lett*. **1974**, 24, 243–248.

[29] R. Everaers. Entanglement effects in defect-free model polymer networks. *New J. Phys.* 1(12), **1999**.

[30] P.J. Flory. *Principles of Polymer Chemistry*. Cornell University Press. **1953**.

[31] D. Frenkel, B. Smit (**2002**) *Understanding molecular simulation*, 2nd. Academic.

[32] V. Galiatsos, *Molecular Simulation Methods for Predicting Polymer Properties*. Wiley. **2005.**

[33] Ulf. W. Gedde. *Polymer Physics*. Springer. **1999.**

[34] J. H. Gibbs and E. A. Dimarzio. Nature of the Glass Transition and the Glassy State. J. *Chem. Phys.* 28 (**1958**), 373.

[35] H. Goldstein. (**1980**). *Classical Mechanics*, 2nd edition. Addison–Wesley.

[36] A. Grosberg. *Theoretical and Mathematical Models in Polymer Research*. Academic Press. **1998**

[37] J. K. Hao and R. A.Weiss. Mechanical behavior of hybrid hydrogels composed of a physical and a chemical network. *Polymer*. **2013**, *54*, 2174. DOI: 10.1016/j.polymer.2013.01.052.

[38] D. Hawkins, C. Cramer, D. Truhlar. Parametrized Models of Aqueous Free Energies of Solvation Based on Pairwise Descreening of Solute Atomic Charges from a Dielectric *Medium. J. Phys. Chem*. 100:19824–19839, **1996**.

[39] D.R. Heine, G. S. Grest, C. D. Lorenz, M. Tsige, and M. J. Stevens. Atomistic simulations of end-linked poly(dimethylsiloxane) networks: structure and relaxation. *Macromolecules*. 37(10):3857-3864, **2004**.

[40] Berk Hess, Carsten Kutzner, David van der Spoel, Erik Lindahl (**2008**). GROMACS 4: Algorithms for Highly Efficient, Load-Balanced, and Scalable Molecular Simulation. *Journal of Chemical Theory and Computation*. 4 (3): 435–447.

[41] B. Hess and et al. *Gromacs*, 4.6 edition. University of Groningen. **2012**.

[42] A. Hiller, F.T. Wall, D.J. Wheeler. Statistical computation of mean dimensions of macromolecules. *J. Chem. Phys.* **1954**, 22, 1036.

[43] Matthew Hoyles, Vikram Krishnamurthy, MaySiksik, Shin-Ho Chung. Brownian Dynamics Theory for Predicting Internal and External Blockages of Tetraethylammonium in the KcsA Potassium Channel. *Biophysical journal*. Volume 94, Issue 2, 15 January **2008**, Pages 366-378

[44] Helgi I. Ingólfsson, Cesar A. Lopez, Jaakko J. Uusitalo, Djurre H. de Jong, Srinivasa M. Gopal, Xavier Periole, Siewert J. Marrink (**2014**). The power of coarse graining in biomolecular simulations. *Wiley Interdisciplinary Reviews: Computational Molecular Science.* 4 (3): 225–248.

[45] Takakazu Ishikura, Tatsuro Hatano, Takahisa Yamato. Atomic stress tensor analysis of proteins. *Chemical Physics Letters*. Volumes 539–540, 29 June **2012**, Pages 144-150.

[46] The Japan Association for Chemical Innovation (JACI), *Computer Simulation of Polymeric Materials*. Springer **2016.**

[47] J. Jagur-Grodzinski (**2009**) Polymeric gels and hydrogels for biomedical and pharmaceutical applications. *Polym Adv Technol* 21:27–47.

[48] Frank Jensen. *Introduction to Computational Chemistry*, 2nd Edition. Wiley. **2006**.

[49] B. Johnson, D.J. Niedermaier, W.C. Crone, J. Moorthy, D.J. Beebe. Mechanical Properties of a pH Sensitive Hydrogel. *Proceedings of the 2002 Society for Experimental Mechanics (SEM) Annual Conference*, Milwaukee, WI, USA. 10–12 June **2002**, pp. 1–2.

[50] R. M. Jones (**2008**). Deformation Theory of Plasticity. Bull Ridge Corporation.

[51] M.N. Khalid, F. Agnely, N. Yagoubi, J.L. Grossiord, G. Couarraze. (**2002**). Water state characterization, swelling behavior, thermal and mechanical properties of chitosan based networks. *European Journal of Pharmaceutical Sciences*. 15, 425–432.

[52] Sebastian Kmiecik, Dominik Gront, Michal Kolinski, Lukasz Wieteska, Aleksandra Elzbieta Dawid, and Andrzej Kolinski (**2016**). Coarse-Grained Protein Models and Their Applications. *Chem Rev.* 2016 Jul 27,116(14):7898-936.

[53] G.H. Ko, M.M. Osias, D.A. Tremblay, M.D. Barrera, C.-C. Chen. Process simulation in polymer manufacturing. *Computers & Chemical Engineering*. Volume 16, Supplement 1, May **1992**, Pages S481-S490.

[54] M. Kotelyanskii and D.N. Theodorou (eds.). *Simulation Methods for Polymers*, Marcel Dekker. **2004**.

[55] H.A. Kramers. Brownian motion in a field of force and the diffusion model of chemical reactions. *Physica.* **1940**, 7, 284–305.

[56] F. Kremer and W. Richtering (eds.). *Intelligent Hydrogels, Progress in Colloid and Polymer Science*. Springer. **2014**, 205-221.

[57] Carsten Kutzner, David Van Der Spoel, Martin Fechner, Erik Lindahl, Udo W. Schmitt, Bert L. De Groot, Helmut Grubmüller (**2007**). Speeding up parallel GROMACS on high-latency networks. *Journal of Computational Chemistry*. 28 (12): 2075–2084.

[58] L.D. Landau, and E.M.Lifshitz. (**1981**). *Theory of Elasticity* 2nd, Pergamon Press

[59] A. Leach. *Molecular Modelling: Principles and Applications*, 2nd Edition. Pearson **2001**.

[60] B.P. Lee, Y. Liu, and S. Konst. Novel hydrogel actuator based on biomimetic chemistry. *MRS Proceedings*. 1710, **2014**.

[61] Soah Lee, Xinming Tong and Fan Yang. Effects of the poly(ethylene glycol) hydrogel crosslinking mechanism on protein release. *Biomater. Sci.* **2016**, 4, 405.

[62] Ben Leimkuhler, Charles Matthews. *Molecular Dynamics.* Springers. **2015**.

[63] Y. K. Leung and B. E. Eichinger. Computer simulation of end-linked elastomers. I. Trifunctional networks cured in the bulk. *J. Chem. Phys.* **1984**, 80, 3877.

[64] Hua Li. *Smart Hydrogel Modelling*. Springer. **2009.**

[65] P. Lin and R. Khare. Molecular simulation of cross-linked epoxy and epoxyposs nanocomposite. *Macromolecules*. 42(12):4319-4327, **2009**.

[66] J. W. Liu, M. E. Mackay, and P. M. Duxbury. Molecular dynamics simulation of intramolecular cross-linking of BCB/styrene copolymers. *Macromolecules*. 42:8534-8542, **2009**.

[67] B. Lu, D. Zhang, J.A. McCammon (Jun **2005**). Computation of electrostatic forces between solvated molecules determined by the Poisson-Boltzmann equation using a boundary element method. *The Journal of Chemical Physics.* 122 (21): 214102.

[68] J. E. Mark. *Physical Properties of Polymers*, 2nd edition. American Chemical Society. **1993.**

[69] Edith Mathiowitz. *Encyclopedia of Controlled Drug Delivery*. Wiley. **1999.**

[70] O. Mazur and I. Oppenheim. Molecular theory of Brownian motion. *Physica.* **1970**, 50, 241–258.

[71] Hamidi Mehrdad, Azadi Amir, Rafiei Pedram. Hydrogel nanoparticles in drug delivery. *Adv Drug Deliv Rev.* **2009**, 60(15):1638–49.

[72] Benedetta Mennucci, Roberto Cammi. *Continuum Solvation Models in Chemical Physics: From Theory to Applications*. Wiley. **2007**.

[73] M. Meunier. *Industrial applications of Molecular Simulations*. CRC Press. **2011.**

[74] Yrr A. Morch, Ivan Donati, Berit L. Strand. Effect of Ca^{2+}, Ba^{2+}, and Sr^{2+} on alginate microbeads. *Biomacromolecules*. **2006** May, 7(5):1471-80.

[75] K. Mukae, M. Sakurai, S. Sawamura, K. Makino, SW. Kim , I. Ueda, K. Shirahama (**1993**) Swelling af poly(N-Isopropylacrylamide) gels an water-alcohol (C1-C4) mixed-solvents. *J. Phys. Chem.* 97(3):737–741.

[76] F. Müller-Plathe, W.F. van Gunsteren (**1997**) Solvation of poly(vinyl alcohol) in water, ethanol and an equimolar waterethanol mixture: structure and dynamics studied by molecular dynamics simulation. *Polymer.* 38(9):2259–2268.

[77] Leena Nebhani, Veena Choudhary , Hans-Jurgen P. Adler, and Dirk Kuckling. pH- and Metal Ion- Sensitive Hydrogels based on N-[2-(dimethylaminoethyl)acrylamide]. *Polymers.* **2016**, 8(6), 233.

[78] O. Okay, S. Durmaz. Charge density dependence of elastic modulus of strong polyelectrolyte hydrogels. *Polymer*. 43(**2002**), 1215–1221.

[79] A. Onufriev, D.A. Case, D. Bashford (Nov **2002**). Effective Born radii in the generalized Born approximation: the importance of being perfect. *Journal of Computational Chemistry*. 23 (14): 1297–304.

[80] A. Onufriev, D. Bashford, D. Case. Exploring protein native states and large-scale conformational changes with a modified Generalized Born model. PROTEINS: *Struct. Funct. Gen*. 55(2):383–394, **2004**.

[81] S. Panprung, R. Uracha, S. Pitt. Preparation and characterization of asiaticoside-loaded alginate films and their potential for use as effectual wound dressings. *Carbohydrate Polymers.* **2011**, 8 3(4):1457–69.

[82] Eric Papas, James S. Wolffsohn and Lyndon Jones. Innovation in contact lenses: basic research and clinical science. *Journal of optometry*. **2010**, 03:123-4.

[83] Linus Pauling. *The nature of the chemical bond and the structure of molecules and crystals: an introduction to modern structural chemistry,* 3rd edition. Cornell University Press. **1960**.

[84] S. Pelzer and D. Hofmann. Structure–property relations between silicon containing polyimides and their carbon containing counterparts. *Mol. Simul*. 34, **2008**, 10–15.

[85] Davit A. Potoyan, Alexey Savelyev, Garegin A. Papoian. (**2013**). Recent successes in coarse-grained modeling of DNA. *Wiley Interdisciplinary Reviews: Computational Molecular Science.* 3 (1): 69–83.

[86] Di Qiu, Peter S. Shenkin, Frank P. Hollinger, and W. Clark Still. The GB/SA Continuum Model for Solvation. A Fast Analytical Method for the Calculation of Approximate Born Radii. *J. Phys. Chem. A.* 101:3005–3014, **1997**.

[87] M. C. Roberts, M. C. Hanson, Massey, E. A. A. P.Karren, P. F. Kiser. Dynamically restructuring hydrogel networks formed with reversible covalent crosslinks. *Adv. Mater.* **2007**, *19*, 2503. DOI: 10.1002/adma.200602649.

[88] R. J. Roe. *Computer simulation of polymers*. Prentice Hall. **1991**

[89] J. P . Ryckaert and A. Bellemans. Molecular dynamics of liquid butane near its boiling point. *Chem. Phys. Lett.* **1975**, 30, 123–125.

[90] A. Sariban and K. Binder, Phase-Separation of polymer mixtures in the presence of solvent. *Macromolecules.* **1988**, 21 (3), pp 711–726.

[91] Justin M. Saul, David F. Williams. *Hydrogels in regenerative medicine, principles of regenerative medicine,* 2nd edition. **2011**. p. 637–61.

[92] C. Schepers and D. Hofmann. Molecular simulation study on sorption and diffusion processes in polymeric pervaporation membrane materials. *Mol. Simul.* 32, **2006**, 2.

[93] T. Schlick. *Molecular modelling and simulation: an interdisciplinary guide*, 2nd edition. Springer. **2010.**

[94] U.P. Schroder, W. Oppermann. (**2002**). Computer simulation of network formation via crosslinking copolymerization. *Macromolecular Theory and Simulations*. 6, 151–160.

[95] S. Seiffert and J. Sprakel. Physical chemistry of supramolecular polymer networks. *Chemical Society Reviews.* **2012**, *41*, 909. DOI: 10.1039/c1cs15191f.

[96] R.D. Shannon (**1976**). Revised effective ionic radii and systematic studies of interatomic distances in halides and chalcogenides". *Acta Crystallogr A.* 32: 751–767.

[97] X. Sun, G. Zhang, Q. Shi, B. Tang, Z.J. Wu. Preparation and characterization of water-swellable natural rubbers. *J Appl. Polym. Sci.* **2002**, 86:3212–717.

[98] E.B. Tadmor, R.E. Miller. *Modeling Materials: Continuum, Atomistic and Multiscale Techniques*. Cambridge University Press. **2011.**

[99] Y. Tamai, H. Tanaka (**1998**). Dynamic properties of supercooled water in poly(vinyl alcohol) hydrogel. *Chem Phys Lett.* 285(1–2):127–132.

[100] P. Taylor and J. Tabachnik. Entropic forces—making the connection between mechanics and thermodynamics in an exactly soluble model. *European Journal of Physics*. 34 (3), **2013.**

[101] L.R.G Treloar. *The Physics of Rubber Elasticity*. Oxford University Press. **1975.**

[102] H. Vale, A. Daiss, O. Naeem, L. Seda, K. Becker, K.-D. Hungenberg. Models in the Polymer Industry: What Present? What Future? *Macromol. Symp*. **2013**, 333, 286–296.

[103] V. Varshney, S. S. Patnaik, A. K. Roy, and B. L. Farmer. A molecular dynamics study of epoxy-based networks: Cross-linking procedure and prediction of molecular and material properties. *Macromolecules*. 41(18):6837-6842, **2008**.

[104] J. Walter, J. Sehrt, J. Vrabec, H. Hasse (**2012**) Molecular dynamics and experimental study of conformation change of poly(n-isopropylacrylamide) hydrogels in mixtures of water and methanol. *J Phys Chem B.* 116(17):5251–5259.

[105] W.A. Wall and F.T.Seitz. Simulation of polymers by self-avoiding, non-intersecting random chains at various concentrations. *J. Chem. Phys*. **1977**, 67, 3722–3726.

[106] J.D. Weeks, D. Chandler and H.C. Andersen. Role of repulsive forces in determining the equilibrium structure of simple liquids. *J. Chem. Phys.* 54 (**1971**), 5237–47.

[107] Horst Weiss, Peter Deglmann. Needs and Opportunities – Molecular Modeling Meets Polymer Process Modeling. *Macromol. Symp.* **2011**, 302, 6–15.

[108] R. Wu, T. Li, and E. Nies. Langevin dynamics simulation of chain crosslinking into polymer networks. *Macromolecular Theory and Simulations*. 21(4):250-265, **2012**.

[109] R. Wu, T. Li, and E. Nies. Polymer networks by molecular dynamics simulation: Formation, thermal, structural and mechanical properties. *Chinese Journal of Polymer Science*. 31:21-38, **2012**.

[110] Hiromasa Yagyu. Coarse-grained Molecular Dynamics Simulation of the Effects of Strain Rate on Tensile Stress of Cross-Linked Rubber. *Journal Soft Materials*. Volume 13, **2015** - Issue 4.

[111] I. Yarovsky and E. J. Evans. Computer simulation of structure and properties of crosslinked polymers: application to epoxy resins. *Polymer*. 43:963-969, **2002**.

[112] W.C. Yount, D.M. Loveless, S.L. Craig. Strong means slow: Dynamic contributions to the bulk mechanical properties of supramolecular networks. *Angewandte Chemie-International Edition.* **2005**, *44*, 2746. DOI: 10.1002/anie.200500026.

[113] W.C. Yount, D.M. Loveless, S.L. Craig. Small-molecule dynamics and mechanisms underlying the macroscopic mechanical properties of coordinatively cross-linked polymer networks. *J. Amer. Chem. Soc.* **2005**, *127*, 14488. DOI: 10.1021/ja054298a.

[114] R. Zhou. Free energy landscape of protein folding in water: explicit vs. implicit solvent. *Proteins.* **2003**, 53 (2): 148–61.